Reconstructing the thermal and exhumation history of the Sierras Pampeanas through low-temperature thermochronology: A case study from the Sierra de Velasco

Andrea L. Stevens Goddard[1,†], **Mariano A. Larrovere**[2,3], **Barbara Carrapa**[1], **R. Hernán Aciar**[4,§], and **Patricia Alvarado**[5]

[1]*Department of Geosciences, University of Arizona, Tucson, Arizona 85721, USA*
[2]*Centro Regional de Investigaciones Científicas y Transferencia Tecnológica La Rioja, Consejo Nacional de Investigaciones Científicas y Técnicas, Anillaco, Argentina*
[3]*Instituto de Geología y Recursos Naturales, Centro de Investigación e Innovación Tecnológica, Universidad Nacional de La Rioja, La Rioja, Argentina*
[4]*Departamento de Geología, Facultad de Ciencias Exactas, Físicas y Naturales, Universidad Nacional de San Juan, San Juan, Argentina*
[5]*Centro de Investigaciones de la Geósfera y la Biósfera, Departamento de Geofísica y Astronomía, Facultad de Ciencias Exactas, Físicas y Naturales, Universidad Nacional de San Juan-Consejo Nacional de Investigaciones Científicas y Técnicas, San Juan, Argentina*

ABSTRACT

The Sierras Pampeanas of Argentina have been used as a classic case study to understand the processes and mechanisms involved in thick-skinned deformation; however, the history of exhumation and uplift of these ranges remains enigmatic. This study presents new thermochronology and field observations from the Sierra de Velasco, one of the highest relief (>4 km) and least studied mountains in the Sierras Pampeanas. Advances in the annealing and diffusion kinetics of the apatite fission track and (U-Th-Sm)/He systems provide the tools to interpret a data set with a complex Carboniferous to Miocene cooling history. Our results show that rocks sampled across 2 km of structural depth have experienced protracted exposure to temperatures at or above ~60 °C from ca. 320 to 120 Ma. The well-constrained thermal history allows us to identify subsequent thermal perturbations including an elevated geothermal gradient during Cretaceous rifting, late Cretaceous–Paleocene cooling due to isothermal relaxation and/or exhumation, and accelerated Miocene exhumation. Quantitative estimates of the minimum rock overburden suggest that 1.0 ± 0.8 km of rock has been eroded from the Sierra de Velasco since the early Miocene. Although a low geothermal gradient (≤25 °C/km) may support the exhumation of Sierra de Velasco coincident with the onset of flat-slab subduction in the late Miocene, we suggest inherited paleotopography existed before the Miocene and possibly since the Paleozoic. Final cooling and exhumation beginning in the early to middle Miocene, concurrent with the onset of flat slab subduction, contributed to the topography observed today, but cannot explain the entirety of the modern relief. We propose that a history of long-lived topography may be extrapolated throughout the Sierras Pampeanas region.

INTRODUCTION

The Sierras Pampeanas region of west-central Argentina between ~27° and 34° S is characterized by crystalline basement-cored block uplifts separated by wide flat plains. Located east of the Cenozoic retroarc fold and thrust belt of the Andean Precordillera, the Sierras Pampeanas represent the inboard extreme of Andean Cordilleran deformation along high-angle reverse faults at distances ~450–650 km from the subduction zone (González Bonorino, 1950) (Fig. 1). The thick-skinned structural style of the region coupled with the initiation of flat slab subduction by the middle to late Miocene have caused the Sierras Pampeanas region to be widely used as a modern analogue for the Laramide region of the western United States (e.g., Jordan and Allmendinger, 1986).

Whereas the prevailing view suggests that the topographic expression of the basement block uplifts of the Sierras Pampeanas is associated with Miocene flat slab subduction (Dávila et al., 2004; Coughlin et al. 1998; Jordan et al., 1989; Dávila and Carter, 2013; Jordan and Allmendinger, 1986), few thermochronometers record Miocene–Pliocene exhumation ages (Jordan et al., 1989; Coughlin et al. 1998; Löbens et al., 2011; Bense et al., 2013; Löbens et al. 2013a, 2013b; Enkelmann et al., 2014; Ortíz et al., 2015). Many workers suggest that the basement rocks of the Sierras Pampeanas were likely exposed at the surface for hundreds of millions of years forming a regional peneplain (Turner, 1971; González Bonorino, 1972), but maintain that the Sierras Pampeanas did not have mountainous topography until the Miocene (Jordan et al., 1984; Dávila and Astini, 2007; Dávila and Carter, 2013). Other studies suggest that the Sierras Pampeanas ranges formed positive topographic features throughout the Paleozoic and into the Mesozoic, were eroded by the end of the Paleogene, and were later uplifted in the Miocene–Pliocene (Jordan et al., 1989). Alternatively, some evidence from the southern Sierras Pampeanas suggests that these ranges have exhibited positive topography since the Paleozoic (Bense et al., 2013) but

have experienced relatively low erosion rates (~0.010–0.024 km/Ma) (Jordan et al., 1989; Löbens et al., 2011; Bense et al., 2013).

The scarcity of sedimentary strata in the Sierras Pampeanas region makes reconstructing the uplift history of the Sierras Pampeanas using geologic field relationships difficult. Whereas Neogene strata are abundant throughout the Precordillera to the west (e.g., Reynolds et al., 1990; Jordan et al., 2001; Ciccioli et al., 2011), they are noticeably absent in the Sierras Pampeanas region. Additionally, pre-Neogene strata that may have covered the ranges if they were buried before Miocene uplift are also scarce (Fisher et al., 2002). Rifting associated with the opening of the South Atlantic Ocean was ubiquitous throughout western Argentina in the mid-late Cretaceous, and evidence of rifting is well preserved in the Salta region ~500 km to the north. Yet, in the Sierras Pampeanas, Cretaceous rift deposits are localized and sparse (Schmidt et al., 1995; Ramos et al., 2002; Fiorelli et al., 2012).

In the northern Sierras Pampeanas, the Sierra de Velasco exhibits high topography (>4 km) with suitable exposures for extensive thermochronological sampling. Geophysical data suggest that steeply dipping reverse faults bound these uplifts on the eastern side of both the western ridge and eastern ridge of the Sierra de Velasco (Fig. 2) and extend to a basal basement décollement at 30 km depth (Alvarado et al., 2005; Alvarado and Ramos, 2011; Richardson et al., 2013). The primary fault of Sierra de Velasco near Anillaco strikes NE-NNE and dips between 44° to 50° to the northwest (Costa, 2008) and the main reverse fault on the eastern side trends NE with an average dip between 40–50°NW. Both faults juxtapose basement rocks over modern sediments confirming that the reverse faults are currently active. Although several studies have applied low-temperature thermochronology to ranges in the Sierras Pampeanas (Jordan et al., 1989; Coughlin et al.1998; Sobel and Strecker, 2003; Löbens et al., 2011; Bense et al., 2013; Löbens et al., 2013a, 2013b; Ortíz et al., 2015), almost no thermochronology data exists in the Sierra de Velasco, one of the highest ranges in the region. Sierra de Velasco is ideal for conducting a thermochronological investigation combining (U-Th-Sm)/He thermochronology on apatite, apatite fission track thermochronology, and thermal-kinetic modeling because the magnitude of exhumation along the hanging wall of the high-angle reverse fault along its western ridge exposes up to 2 km of structural relief.

The paleogeography of the Sierras Pampeanas since the Paleozoic has important implications for the multiple tectonic processes that

have affected this region. The sensitivity of low temperature thermochronometers to changes in temperature due to both burial and exhumation makes this approach ideal for reconstructing the geologic history of the Sierra de Velasco and reconstructing the paleogeography of the region. By combining multiple thermochonometers on samples taken throughout the Sierra de Velasco, this study will test the following models: (1) the region has had little to no topography until the late Miocene; (2) some paleotopography was established by the middle Paleozoic that persisted until the early Neogene with some possible reactivation in the Cretaceous–Paleogene and accelerated exhumation in the late Miocene. The results of this work will provide a better understanding of the tectonic processes responsible for exhumation and uplift of the Sierra de Velasco including the role of Miocene flat slab subduction, the inboard propagation of deformation, and the role of inherited structures in the Sierras Pampeanas.

GEOLOGIC SETTING

Tectonic Setting

The igneous and metamorphic rocks of the Sierra de Velasco, as well as much of the basement block uplifts exposed in the eastern Sierras Pampeanas, have ages that correspond to the Ordovician–Silurian Famatinian orogeny and the tectono-magmatic Carboniferous event (de los Hoyos et al., 2011; Dahlquist et al., 2013) that developed along the proto-Andean margin of Gondwana. The Famatinian belt was a subduction-related orogeny and the granitoid rocks of the Sierra de Velasco were part of the main magmatic arc during Ordovician times (Grosse et al., 2011). Granitoids were deformed by large NNW-striking reverse ductile shear zones that extend along the Sierra de Velasco (Larrovere et al., 2016). During the early Carboniferous, A-type plutons attributed to an extensional retro-arc tectonic setting (Alasino et al., 2012) were emplaced throughout the older Famatinian arc system.

It is likely that the Sierra de Velasco was exposed to several periods of rifting prior to Andean orogenesis. During the Late Permian to Triassic, extensional basins formed to the west of the Sierra de Velasco in the Ischichuca and Villa Unión areas (Fig. 1) from between ca. 290 and 240 Ma (Fernandez-Seveso and Tankard, 1995). Between 100 and 200 m of the Carboniferous to Permian strata of the Libertad and Sauces formations are exposed near the town of Sanagasta (Fig. 2) in east-central Sierra de Velasco (Pieroni and Georgieff, 2007) and along the western side of the southernmost tip of this

range (Los Colorados area). Carboniferous to Permian strata rest unconformably on basement rocks and field measurements document dips 15°–20° to the west (Fig. 2). Reconstructions of the depositional relationship between sedimentary strata and the underlying basement summarized in Figure 2 assume that strata are undeformed and horizontal at deposition. Cretaceous rift deposits associated with the Salta Rift and the opening of the South Atlantic are well preserved in the Eastern Cordillera of NW Argentina to the north of the study area (Reyes and Salfity, 1973; Galliski and Viramonte, 1988; Salfity and Marquillas, 1994) whereas time equivalent deposits are sparse in the study area (Fiorelli et al., 2012). Upper Cretaceous rifting associated with the Salta Rift has been recorded using low temperature thermochronology within the transition zone between the Eastern Cordillera and the Sierras Pampeanas (Mortimer et al., 2007; Carrapa et al., 2014). These studies suggest the presence of Cretaceous paleotopography associated with rift-flank uplift (Sierras de Quilmes) which was never buried deeply enough to thermally reset the apatite fission track and helium systems during Cenozoic foreland basin development (Fig. 1). Salfity and Marquillas (1994) suggest that Cretaceous paleotopography could have involved a Pampean Arch that included present-day Sierra de Velasco. Near the Sierra de Velasco, the Cretaceous Los Llanos Formation, notable for its dinosaur egg fossils clustered along syndepositional hydrothermal vents (Grellet-Tinner and Fiorelli, 2010; Fiorelli et al., 2012), may record Cretaceous rifting (Fiorelli et al., 2012). Here, an angular unconformity separates Carboniferous to Permian strata (10°–15°) from the Los Llanos Formation (Fig. 2). However, the Los Llanos Formation is exposed in the Sierra de Velasco only near Sanagasta, and the depositional setting remains enigmatic. In the southern Sierras Pampeanas, preserved Cretaceous rift deposits define a period of extension between ca. 120 and 90 Ma (Schmidt et al., 1995; Ramos et al., 2002). These deposits are mostly associated with localized depocenters and the original extent of a regional Cretaceous rift basins remains unconstrained (Schmidt et al., 1995).

The post-Cretaceous sedimentary record is also scarce. No Paleogene strata are recognized in Sierra Velasco. Upper Miocene sedimentary rocks of the Salicas Formation can be found along the northwestern boundary of the Sierra de Velasco and rest unconformably over basement rocks with an average dip of ~13° to the west (Tauber, 2005) (Fig. 2). The sparse sedimentary record makes it difficult to reconstruct both the spatiotemporal distribution of Cretaceous extension throughout most of the Sierras Pampeanas region and the timing of regional uplift.
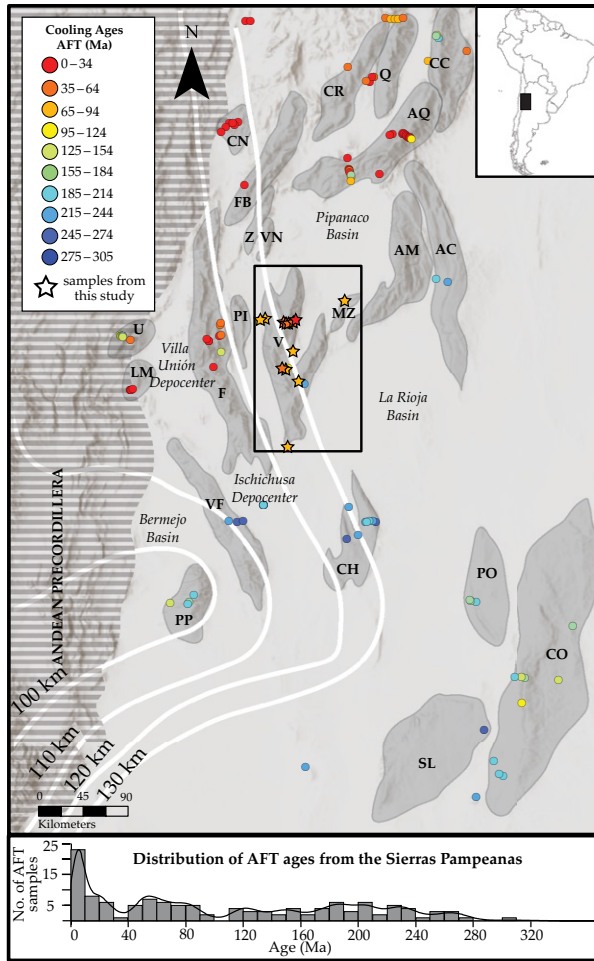
Figure 1. Regional map of the Sierras Pampeanas with apatite fission track (AFT) cooling ages from this work (stars) and previous studies (circles) color coded by cooling age. Modern depth to slab after Anderson et al. (2007) and Cahill and Isacks (1992) is shown by white lines. The Sierras Pampeanas are outlined in gray. CR—Sierra de Chango Real; Q—Sierra de Quilmes; CC—Cumbres Calchaquíes; AQ—Sierra de Aconquija; CN—Cerro Negro; FB—Sierra de Fiambalá; Z—Sierra de Zapata; VN—Sierra de Vinquis; AC—Sierra de Ancasti; AM—Sierra de Ambato; MZ—Sierra de Mazán; V—Sierra de Velasco; PI—Sierra de Paimán; F—Sierra de Famatina; U—Sierra de Umango; LM—Sierra de Maz; VF—Sierra de Valle Fértil; PP—Sierra de Pie de Palo; CH—Sierra de Chepes; PO—Sierra de Pocho; SL—Sierra de San Luis; CO—Sierras de Córdoba. A histogram and kernel density estimate of the 125 AFT dates shown in Figure 1 are plotted on the bottom of the figure. Sources are listed in the text.
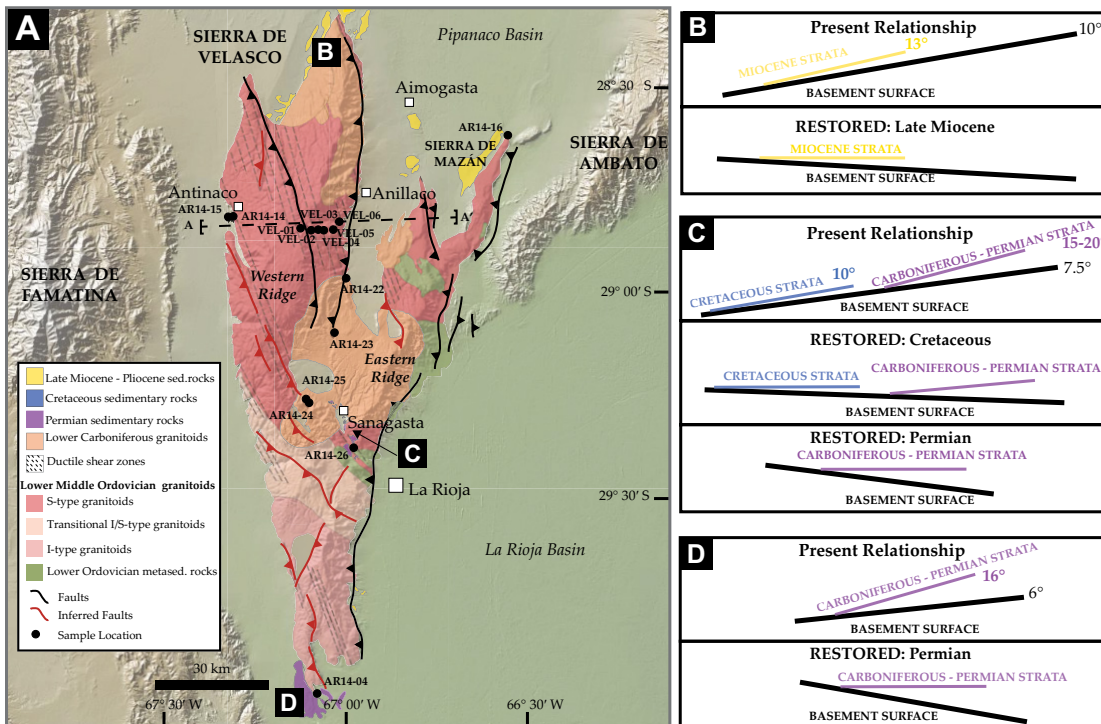

Figure 2. Geologic map of Sierra de Velasco (A) with sample locations indicated by black circles. Restored Miocene, Cretaceous, and Carboniferous strata locations are shown on (A) with rotations shown in (B), (C), and (D). Location of cross section A–A′ shown in Figure 3 is indicated.

Existing Thermochronological Data

Existing thermochronological ages from throughout the Sierras Pampeanas, including the Sierra de Velasco, show mixed results (Fig. 1). Regional apatite fission track (AFT) cooling ages range from Permian to Pliocene in age, but the majority of AFT samples, 51%, record Mesozoic cooling ages. Approximately 26% of cooling ages are Neogene in age, coincident with the latest period of flat slab subduction predicted by Yáñez et al. (2001). Of the remaining AFT samples, 17% are Paleogene and 6% are Paleozoic. The apatite helium (AHe) system is more difficult to evaluate as cooling ages of grains within a sample may vary; however, this system also records a range of cooling ages from Permian to Pliocene (Löbens et al., 2011; Bense et al., 2013; Löbens et al. 2013a; Löbens et al., 2013b; Enkelmann et al., 2014; Ortíz et al., 2015).

The distribution of apatite thermochronology cooling ages exhibits a clear regional trend. Miocene AFT ages in the Sierras Pampeanas are more common in the northern ranges (Sierra de Quilmes, Sierra de Aconquija, Cerro Negro) (Mortimer et al., 2007; Carrapa et al., 2006, 2014; Löbens et al., 2013b) and western ranges (Sierra de Famatina, Sierra de Maz) (Coughlin et al., 1998) which also correspond to some of the highest elevations in the Sierras Pampeanas (Fig. 1). Samples from the northern Sierras Pampeanas also preserve a record of Cretaceous cooling which is interpreted as exhumation of paleorift flanks (Mortimer et al., 2007; Carrapa et al., 2014). In the southern Sierras Pampeanas, Cretaceous thermochronology cooling ages (apatite fission track, zircon, and apatite helium) are also associated with Cretaceous rifting (Bense et al., 2013). Evidence of Paleozoic–Mesozoic cooling signals is prevalent throughout the Sierras Pampeanas including the northern and western ranges, but these older cooling signals dominate the southern and eastern ranges (Fig. 1).

Coughlin et al. (1998) used AFT thermochronology to suggest four periods of cooling. A Carboniferous to Permian (300–280 Ma) cooling event and an early Jurassic to middle Jurassic (200–174 Ma) cooling event were interpreted to represent early exhumation. These ages are supported by AHe data and thermal modeling in the southern Sierras Pampeanas ranges (Bense et al., 2013; Enkelmann et al., 2014). Later Andean exhumation, according to Coughlin et al. (1998), is recorded by AFT Paleocene–Eocene and late Miocene cooling ages. Extrapolating the cooling history recorded by apatite thermochronometers to interpret the timing of regional uplift proves contro-

versial. The prevailing view is that despite the paucity of Miocene apatite thermochronology cooling ages, regional uplift of the Sierras Pampeanas ranges was concentrated mainly in the Miocene coincident with flat slab subduction (Carrapa et al., 2006, 2008; Löbens et al., 2013a, b) and that a low geothermal gradient limited the record of rapid Miocene exhumation using low temperature thermochronology (Dávila and Carter, 2013); however, new measurements using thermochronology data place the Miocene geothermal gradient between 25 °C/km and 35 °C/km (Stevens Goddard and Carrapa, 2017) and raise skepticism about this exhumation model. Some evidence suggests that positive topography in the southern Sierras Pampeanas (e.g., Sierras de Córdoba, Sierra de Pocho, Sierra de San Luis) may predate the Neogene (Bense et al., 2013), but this hypothesis has not been extended to northern ranges.

METHODS

Apatite thermochronology, using both cooling dates and thermal modeling, is uniquely suited to constrain the time-temperature history of these samples and the exhumation of the upper ~5–7 km of the Earth's crust. This study collected samples for apatite thermochronology by targeting the hanging wall of faults along the eastern and western sides of the western ridge of the Sierra de Velasco including Lower Ordovician and Lower Carboniferous granitoids with minimal weathering surfaces (Fig. 2). We collected a suite of six samples along strike of a major reverse fault lineament and six samples from a vertical profile on the eastern side of the western ridge of the Sierra de Velasco near Anillaco, a location of high topography that likely experienced maximum exhumation in the range (Fig. 2). Two samples from faults along the western side of the Sierra de Velasco near Antinaco and one sample east of the Sierra de Velasco in the Sierra de Mazán were collected for comparative purposes. Sampling locations are summarized in Table 1 and in Figure 2.

Apatite Fission Track Thermochronology

Apatite fission track (AFT) thermochronology is based on the natural fission of ^{238}U atoms in an apatite grain (Price and Walker, 1963). The complete retention of fission tracks constrains the timing of mineral exposure to temperatures below 120–80 °C (Green et al., 1989). At temperatures between 120 and 80 °C, a range known as the partial annealing zone (PAZ) (Fleischer et al., 1975; Wagner et al., 1989), fission tracks begin to anneal. Above these temperatures of the PAZ, fission tracks are not preserved. When

fission tracks first form in apatite, they have a length of ~15 μm after etching (Fleischer et al., 1975). Exposure to temperatures in or above the PAZ systematically shortens track lengths (Donelick et al., 1999); consequently, the distribution of track lengths provides an important constraint on the sample's thermal history. Methods for age determination and length measurements reported in Table 1 are included in the Data Repository[1].

Apatite Helium Thermochronology

The (U-Th-Sm)/He system in apatite (AHe) measures radiogenic ^{4}He derived from radioactive decay of ^{238}U, ^{235}U, ^{232}Th, and ^{147}Sm (Farley et al., 1996; Ehlers and Farley, 2003). Although He retentivity depends on many factors, in general, at temperatures above 40–60 °C, ^{4}He diffuses through and is lost from apatite at relatively high rates (Farley et al., 1996), while at temperatures below 40–60 °C, the nominal closure temperature of the system for typical orogenic cooling rates, ^{4}He is largely retained (Farley et al., 1996). At temperatures between 40 and 80 °C, radiogenic production and diffusive loss of ^{4}He may have similar rates, and this temperature range is called the partial retention zone (PRZ) (Farley et al., 1996). The closure temperature of apatite is sensitive to apatite grain size, chemical composition, and extent of radiation damage accumulation (Farley, 2000; Flowers et al., 2009; Gautheron et al., 2013; Fox and Shuster, 2014). The ages observed in a suite of apatite grains from a sample that experienced the same thermal history may thus be different. This reflects the variations in closure temperature of the grains. For samples where the cooling date and effective uranium concentration (eU) display a positive correlation, the cooling date-eU relationship can be exploited using thermal modeling to constrain the time-temperature history of the sample (Flowers et al., 2009). For this reason, we analyzed a minimum of five apatite grains per sample following methods described in the Data Repository (see footnote 1).

The annealing kinetics of an apatite grain provide a key control on the cooling date recorded in the AHe system (Farley, 2000; Flowers et al., 2009; Gautheron et al., 2013; Fox and Shuster, 2014). Typically, the parameter that describes resistance to annealing, r_{mr0}, is assumed to be ~0.83 for the AHe system. (Ketcham et al., 2007b; Gautheron et al., 2013); however, the chemical composition of a grain, specifically a high Cl content, has been shown to alter the

---

TABLE 1. APATITE THERMOCHRONOLOGY AND GEOCHEMISTRY RESULTS

Sample	Latitude	Longitude	Elevation	AFT results				Microprobe results		AHe results		
				Central AFT age (Ma)	Error ±2σ (Ma)	Mean length (μm)	Mean D_{par} (μm)	Mean F content (wt%)	Mean Cl content (wt%)	AHe corrected age (Ma)	Error (±1σ) (Ma)	eU (ppm)
VEL-01	−28.8414	−67.1108	3800	48.91	4.54	10.51	2.32	–	–	91.23	1.29	49.35
										163.72	2.38	60.34
										165.29	2.42	70.21
										199.72	2.80	67.60
										170.33	2.42	54.02
VEL-02	−28.8467	−67.0908	3700	61.47	6.21	12.13	1.69	–	–	211.32	2.98	16.80
										147.36	2.83	13.63
										420.08	6.66	7.56
										164.93	4.62	7.04
										176.37	4.48	12.37
VEL-03	−28.8458	−67.0756	3450	62.55	5.85	10.94	1.95	–	–	230.60	3.26	72.99
										357.77	5.34	5.89
										259.65	3.77	76.40
										240.46	3.56	80.60
										258.52	3.68	87.34
VEL-04	−28.8489	−67.0615	3100	–	–	–	–	–	–	236.64	3.30	76.92
										249.77	3.50	105.42
										235.63	3.38	107.25
										242.66	3.76	47.61
										313.21	5.08	123.01
VEL-05	−28.8442	−67.036	2650	59.81	5.54	10.76	1.86	–	–	185.42	2.88	70.00
										141.60	2.17	70.40
										189.35	3.03	66.90
										181.57	2.78	52.23
										160.39	2.59	92.43
VEL-06	−28.831	−67.0195	1900	18.61	2.24	10.52	2.15	–	–	67.40	1.14	70.89
										384.24	6.01	84.62
										250.38	3.97	59.26
										55.19	0.89	88.21
										74.75	1.43	85.46
										796.27	13.93	68.67
										98.25	1.64	73.63
										229.64	4.17	64.90
										33.13	0.88	40.24
										202.74	3.36	74.57
AR14-22	−28.9728	−67.0027	1590	–	–	–	–	–	–	352.79	5.35	30.01
										390.28	6.29	14.03
										670.48	10.27	11.42
										270.25	4.20	11.44
										435.80	6.38	26.88
AR14-23	−29.1048	−67.0344	1500	71.55	6.63	12.21	2.49	3.19	0.008	249.87	4.28	143.51
										267.20	4.58	113.38
										294.80	5.06	95.43
										883.10	15.84	95.03
										214.24	3.62	88.07
AR14-24	−29.2744	−67.1043	1550	92.3	9.72	11.74	1.82	3.26	0.006	173.29	2.53	33.80
										272.38	4.69	31.17
										124.02	1.96	14.69
										228.01	3.32	33.47
										186.05	3.87	64.21
AR14-25	−29.2649	−67.1126	1820	61.3	6.11	11.28	2.29	3.111	0.008	123.83	3.08	23.01
										72.67	1.76	17.95
										163.17	2.70	39.17
										155.73	2.74	37.40
										107.13	2.21	26.79
AR14-26	−29.3826	−66.9818	880	75	7.33	11.57	2.46	3.134	0.005	210.50	3.64	32.95
										226.70	3.94	50.48
										211.64	3.59	26.75
										221.58	3.37	45.66
										222.95	3.42	58.86
AR14-14	−28.8227	−67.3129	1180	67.41	7.42	–	–	–	–	144.02	2.52	33.80
										152.83	2.56	31.17
										162.60	2.80	14.69
										159.46	2.96	33.47
										365.79	6.31	64.21
AR14-04	−29.974	−67.0822	580	67.25	6.69	11.63	2.12	2.96	0.134	–	–	–
AR14-15	−28.8237	−67.3265	1170	78.56	7.85	–	–	–	–	–	–	–
AR14-16	−28.6481	−66.5655	680	91.13	13.08	–	–	–	–	–	–	–

Note: AFT—apatite fission track; AHe—apatite helium; eU—effective uranium concentration.

r_{mr0} value used for the AHe system (Gautheron et al., 2013; Fox and Shuster, 2014; Ault et al., 2015). To test if high Cl content controlled the annealing parameter, r_{mr0}, values assumed for the apatites from the Sierra de Velasco, we collected compositional data using electron microprobe analysis for five samples, including the four samples modeled from eastern side of the western ridge of the Sierra de Velasco (Table 1). Methods for microprobe analysis are included in the Data Repository.

Thermal Modeling

Modeling in this study employs the HeFTy software program (Ketcham, 2005) which uses thermochronology data to (1) evaluate the likelihood of a proposed time temperature history (forward model) and (2) find a specified number of likely time temperature histories by generating and evaluating large suites of time temperature histories (inverse model). Model inputs include the age, length, and D_{par} (fission track etch pit geometry measurements) data from the AFT system and the age, grain size, and eU data from the AHe system. For AHe sample calibration, we use the radiation damage accumulation and annealing model (RDAAM) calibration model (Flowers et al., 2009) which predicts that protracted exposure to temperatures at or below the PRZ will produce a range of cooling ages as a function of eU, and we use the alpha ejection correction from Ketcham et al. (2011). For AFT samples we use the annealing model outlined in Ketcham et al. (2007a, b). In this study we produce both forward and inverse models for key samples in the Sierra de Velasco to most accurately refine the regional time-temperature history. Details of forward and inverse modeling are described in the Thermal Modeling Results section below.

AFT AND AHe RESULTS

Apatite helium dates (Table 1) from Ordovician and Carboniferous basement of the Sierra de Velasco range from the Lower Permian (294.8 ± 5.1 Ma, sample AR14-23) to early Oligocene (33.1 ± 0.9 Ma, sample VEL-06) excluding twelve grains that have cooling dates older than the Carboniferous (Table 1). Of the remaining 53 grains, 41 grains record dates ranging from the Permian through the Jurassic (ca. 295–147 Ma); ten grains show Cretaceous cooling ages (ca. 144–67 Ma) (Table 1). Two grains have Paleogene cooling dates (55.2 ± 0.9 Ma, 33.1 ± 0.9 Ma). Both grains with Paleogene cooling dates come from sample VEL-06 which is located at the base of the Sierra de Velasco vertical transect in the hanging wall of a major

reverse fault (Table 1; Fig. 3). For most samples, the grains within a single sample exhibit similar cooling dates; however, we note that samples with internal consistency also contain low variability of eU (difference of less than ~30 ppm) among grains of a single sample. Three samples contained grains with significant age differences (>50 my). AHe cooling dates do not correlate with changes in elevation (Fig. 3).

For samples that have both AFT and AHe data, the AFT and AHe cooling dates are inverted with AFT dates that are consistently younger than AHe ages (Table 1). The majority of AFT cooling ages range from the latest Cretaceous to the early Eocene (ca. 92–49 Ma). Track lengths measured from AFT samples exhibit a unimodal distribution with mean track lengths between 12.7 µm and 13.8 µm, corrected for c-axis orientation (Ketcham et al., 2007b) (Table 1). These samples are consistent with structural geology where samples dated in the hanging wall of a fault are younger than AFT dates in the footwall of the fault (Fig. 3). Samples from the vertical transect produce Paleocene–Eocene cooling ages with the exception of the sample located at the base of the vertical transect that records a Miocene cooling age of 18.9 ± 2.19 Ma (Fig. 3).

Four out of five samples including AR14-23, AR14-24, AR14-25, and AR14-26, produced average Cl content (from ten spots) below the detectable level of 0.016%, although some constituent analyses registered above detectable levels (Table 1). One sample, AR14-04, produced average Cl content of 0.134% significantly above the detectable level.

THERMAL MODELING RESULTS

Both forward and inverse modeling provides contributions to the time-temperature history of the Sierra de Velasco. The complexity of this data set, including the inverted AHe and AFT ages and the wide range of AHe dates, favors an integrated modeling approach. We adopt a four step workflow outlined in Figure 4 that utilizes both forward and inverse modeling of AHe and AFT data to identify the most likely time-temperature history of these samples. We note that this work flow is most useful where the AHe system is represented by grains with a sufficient range of eU to exhibit a clear trend. From our observations, a range of at least 40–50 ppm works best to identify these trends.

We begin by modeling the AHe ages from samples located on the east of the Sierra de Velasco, excluding samples taken from the vertical transect, together. Modeling these samples together assumes that the samples have a similar thermal history. This assumption is reasonable because the samples are all from or nearby Carboniferous granitic intrusions and are located at a similar structural depth in relation to faulting along the east side of the Sierra de Velasco with a maximum difference in modern elevation of less than 1 km.

In Step 1 of modeling, we simulate simple time-temperature paths to evaluate the predicted AHe age-eU distribution for each thermal history (Fig. 5). Both the geologic history and the distribution of AHe dates allow us to make three basic assumptions about the time-temperature
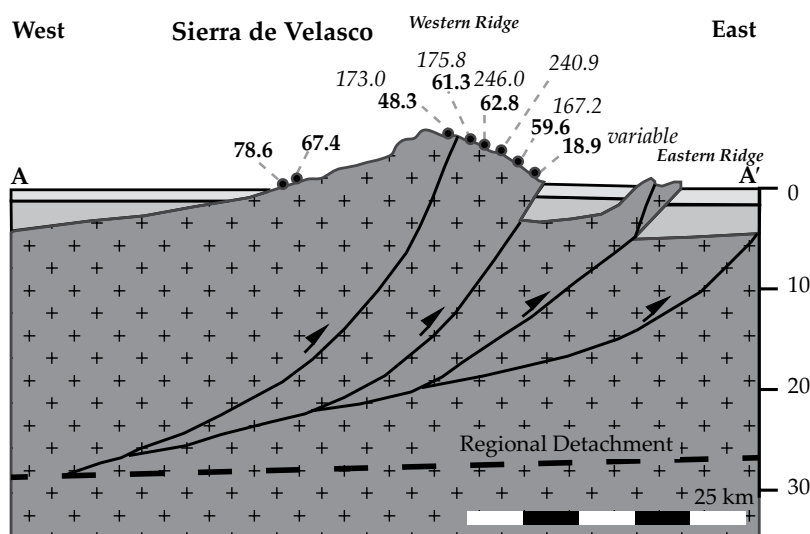

Figure 3. Cross section A–A′ of Sierra de Velasco after Alvarado and Ramos (2011) with thermochronology sample locations and results. Apatite fission track ages are indicated in bold font in rectangles and the weighted mean apatite helium cooling ages are indicated in italics in ovals. Samples with a wide range of cooling ages (variable) are not listed.
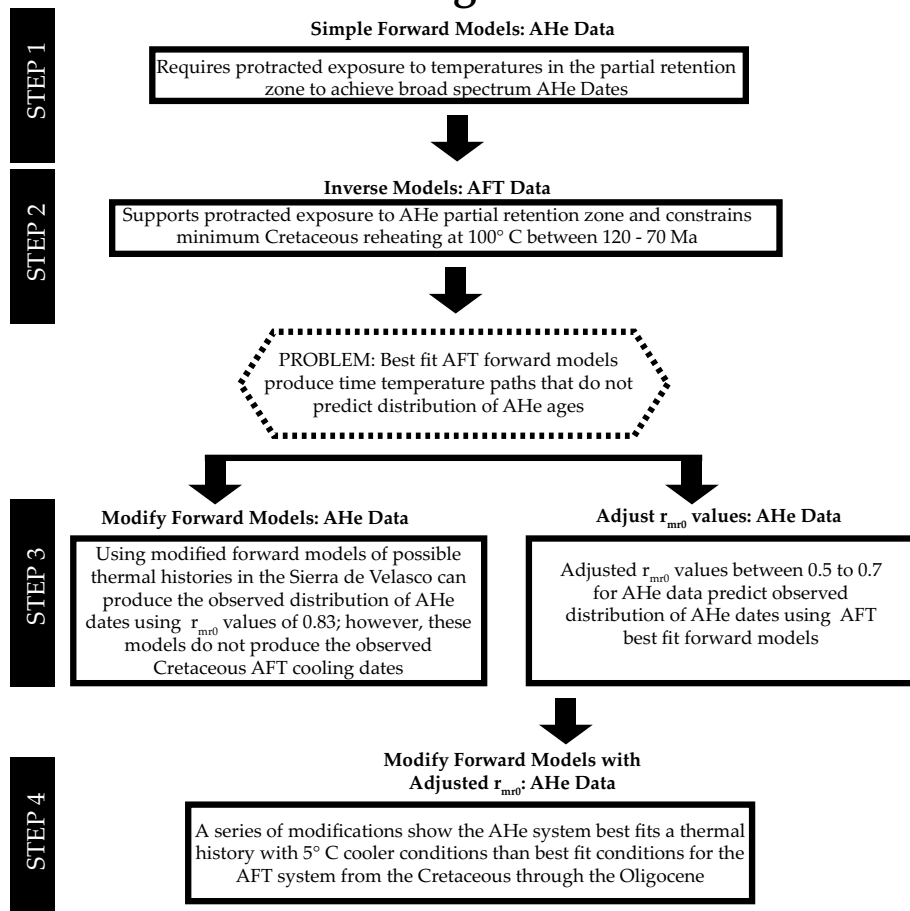
Modeling Process

STEP 1

Simple Forward Models: AHe Data

Requires protracted exposure to temperatures in the partial retention zone to achieve broad spectrum AHe Dates

STEP 2

Inverse Models: AFT Data

Supports protracted exposure to AHe partial retention zone and constrains minimum Cretaceous reheating at 100° C between 120 - 70 Ma

PROBLEM: Best fit AFT forward models produce time temperature paths that do not predict distribution of AHe ages

STEP 3

Modify Forward Models: AHe Data

Using modified forward models of possible thermal histories in the Sierra de Velasco can produce the observed distribution of AHe dates using r_{mr0} values of 0.83; however, these models do not produce the observed Cretaceous AFT cooling dates

Adjust r_{mr0} values: AHe Data

Adjusted r_{mr0} values between 0.5 to 0.7 for AHe data predict observed distribution of AHe dates using AFT best fit forward models

STEP 4

Modify Forward Models with Adjusted r_{mr0}: AHe Data

A series of modifications show the AHe system best fits a thermal history with 5° C cooler conditions than best fit conditions for the AFT system from the Cretaceous through the Oligocene

Figure 4. Thermal modeling work flow. AFT—apatite fission track; AHe—apatite helium; r_{mr0}—annealing parameter.

history of these samples: (1) high heat flow from granitic intrusions in the Carboniferous (de los Hoyos et al., 2011; Dahlquist et al., 2013) overprinted any previous thermal history and constrain the earliest possible records of cooling; (2) the wide range of AHe cooling dates suggests protracted exposure to temperatures in or above the PRZ sufficient to induce crystal damage that increases He retentivity (Flowers et al., 2009); and (3) modern seismic activity of faults in the Sierra de Velasco (Alvarado and Ramos, 2011) suggests uplift-induced cooling occurred in the late Cenozoic.

A suite of ten simple models exploring the timing and temperatures of these assumptions are available in the Data Repository (see footnote 1). We have selected four representative time-temperature histories in Figure 5 that best illustrate the effects of the timing of rapid cooling and the magnitude of the protracted residence temperature on the AHe dates. These generalized scenarios include: (A) steady cooling from the Carboniferous to the Pliocene; (B) rapid Carboniferous cooling followed by protracted exposure to temperatures of 120 °C with final cooling in the Miocene; (C) rapid Carboniferous cooling followed by protracted exposure to temperatures of 70 °C with final cooling in the Miocene; and (D) rapid Permo–Triassic cooling followed by protracted exposure to temperatures of 70 °C with final cooling in the Miocene. Only scenarios C and D provide a range of cooling dates with a positive age-eU trend required by the data in this study (Fig. 5). This age distribution is produced by protracted exposure to temperatures at 70 °C before final Miocene cooling suggesting
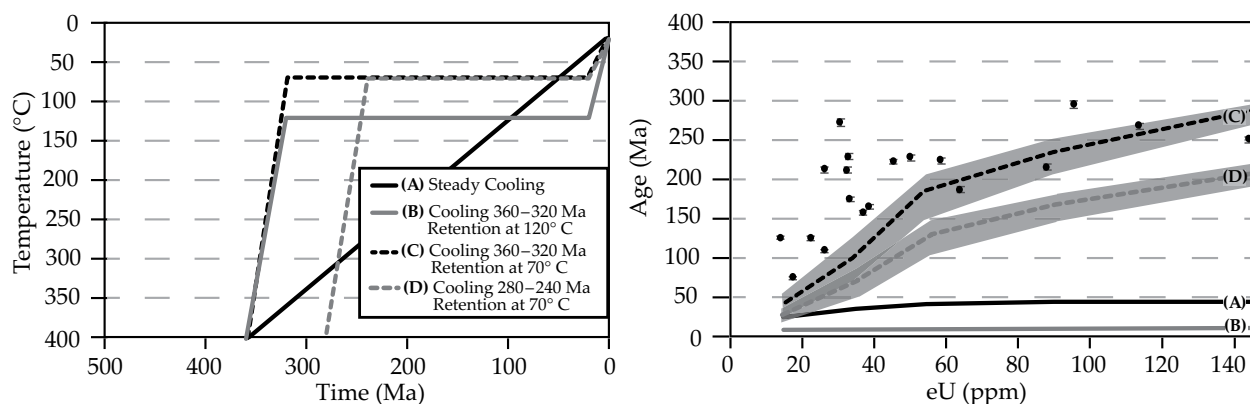

Figure 5. Step 1 of the modeling process uses forward modeling to constrain the time-temperature history of apatite helium (AHe) samples (left). Four simple forward models of time-temperature histories indicated by lines A–D. Additional simple forward models can be found in the Data Repository (see footnote 1). The predicted AHe cooling ages, given these time-temperature histories, are shown by the corresponding envelopes A–D in the right diagram. The observed AHe cooling ages and effective uranium concentration (eU) values from samples in the Sierra de Velasco are indicated in black circles on the right diagram. The time-temperature history C (black dashed line) most closely matches the data from Sierra de Velasco suggesting samples must have been exposed to relatively low temperatures (<60 °C) for a protracted period of time to produce the observed ages. This observation is used in the next step of the modeling process.

long-term residence in the AHe partial retention zone at maximum temperatures ~70 °C. Of these two models, C provides the best fit to the observed data with a range of cooling ages between ca. 40 Ma and 300 Ma indicating that cooling to temperatures in or below the PRZ most likely occurred soon after the emplacement of Carboniferous granitoids (de los Hoyos et al., 2011; Dahlquist et al., 2013).

We use observations from Step 1 to guide Step 2 which produces a series of inverse models from AFT data (Fig. 6). We use the simplistic time-temperature histories in Step 1 to justify a modeling constraint that requires rapid cooling in the Carboniferous and protracted exposure to temperatures cooler than 120 °C at some point between 300 and 100 Ma. Details of inverse modeling are provided in the Data Repository (see footnote 1).

The inverse models from four AFT samples (AR14-23, AR14-24, AR14-25, AR14-26) from the eastern side of the western ridge of the Sierra de Velasco produce similar results. Good fit paths from all samples support protracted exposure to temperatures within and above the AHe PRZ between 40 and 60 °C. Inverse modeling of AFT data also provides useful constraints on the timing and magnitude of latest

Cretaceous reheating observed in AFT cooling dates. This cooling event, likely initiating as early as 120 Ma and continuing no later than 70 Ma requires temperatures, at minimum, of ~100 °C but theoretically could have reached much higher temperatures. Maximum heating during this event is constrained by the diffuse AHe cooling ages that indicate only partial resetting. The magnitude and timing of this event are specifically probed in the integrated forward models combining both the AHe and AFT data later in Step 4 of the modeling process.

Step 1 and Step 2 identify key attributes of the thermal history of these samples in Sierra de Velasco. Specifically, this locale experienced protracted cooling throughout the Paleozoic and most of the Mesozoic with renewed heating in the latest Cretaceous. However, the best fit paths derived from inverse AFT modeling predict AHe cooling ages between ca. 45–10 Ma which do not match the wide spread of observed AHe cooling dates. Attempts at both forward and inverse modeling of AFT and AHe data together fail to produce a thermal history that satisfies both data sets. The main problem here is the difficulty of heating AFT samples to a sufficient temperature so that they record Cretaceous cooling without resetting the AHe system.

We observe that protracted exposure to low temperatures created extensive radiation damage in our apatite samples. In turn, this damage increased the retentivity of helium in the AHe system without affecting the annealing kinetics of the AFT system (Flowers et al., 2009). Such a scenario would effectively raise the closure temperature of the AHe system. However, this relationship alone, which is accounted for in the thermal models using RDAAM for the AHe system (Flowers et al., 2009) does not provide a time-temperature history to fit both the observed AFT and AHe data in the Sierra de Velasco. We address this apparent discrepancy between data sets by investigating the annealing parameters that control the closure temperature of the AHe system. Previous studies by Fox and Shuster (2014) and Ault et al. (2015) have shown that in cases of apatite with high radiation damage, the exposure to temperatures within and above the PRZ does not always restore diffusion kinetics to pre-damage values as predicted by existing He diffusivity models including RDAAM. Prolonged exposure to temperatures at or below the PRZ may have produced high levels of radiation damage in the rocks of the Sierra de Velasco that do not conform to existing radiation damage annealing models.

To test this hypothesis, in Step 3 we modify the parameter that controls damage in the AHe system, r_{mr0} (Fig. 7). The value of r_{mr0} used while modeling the AHe system thus far has been based on the experimentally derived value common in most apatites, ~0.83. Modification of this value to 0.70 and 0.60 as shown in Figure 7 produces a distribution of AHe dates and eU values that begins to resemble the observed data from eastern side of the western ridge of Sierra de Velasco. Whereas both values generally resemble the distribution of AHe cooling ages, an r_{mr0} value of 0.6 best fits the data set. We adopt 0.60 as an estimate of r_{mr0} in our samples for forward modeling in Step 4.

The final step of thermal modeling, Step 4, uses forward models to modify the best fit thermal history from Steps 2 and 3 to better fit the observed AHe age-eU distribution (Fig. 8). First, we assume a constant residence temperature between 60 and 40 °C following Carboniferous cooling to Cretaceous heating. A residence temperature of 40 °C best fits the AHe data. Next we evaluate the Cenozoic residence temperature between Cretaceous cooling at 40 Ma and final Miocene cooling at 20 Ma at temperatures of 80 °C, 75 °C, and 70 °C. A temperature of 70 °C best fits the AHe data (Fig. 8). Finally, we evaluate the magnitude of Cretaceous heating. Maximum heating of 105 °C, 100 °C, and 95 °C produce remarkably different results considering the small range of temperature difference.
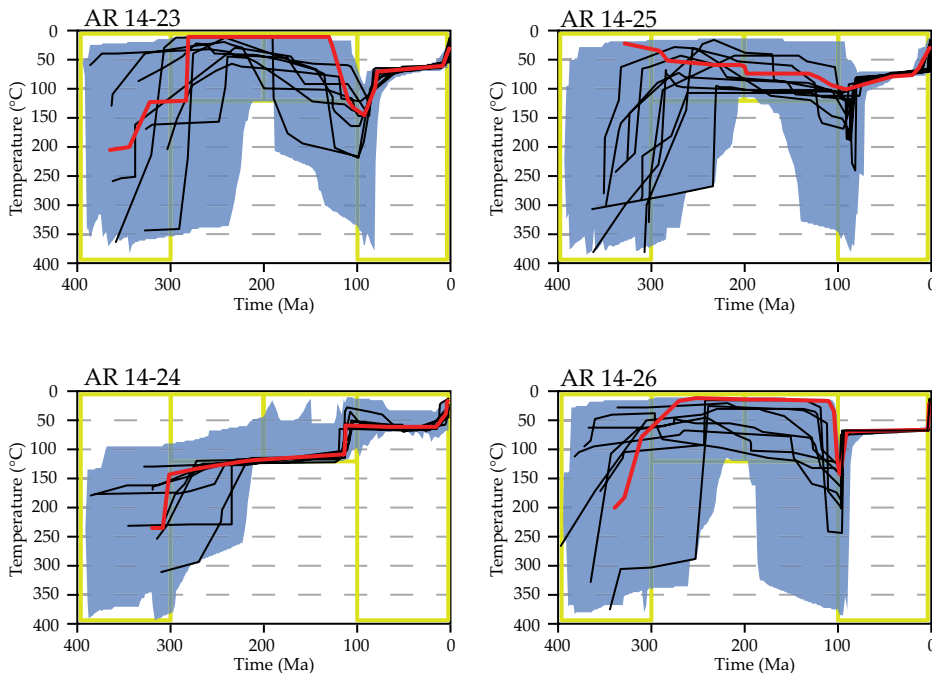

Figure 6. Step 2 of the modeling process uses the observation from Step 1 (Fig. 5) that samples must have experienced low temperatures for a protracted period of time to place constraints on inverse models of the apatite fission track system. Modeling constraints are indicated by yellow boxes. Blue polygons indicate the best fit envelope for 100,000 model runs. The top ten good fit paths are indicated by black lines. A red line shows the best fit path for each sample. A generalized best fit path from these models is used in Step 3 of the modeling process.
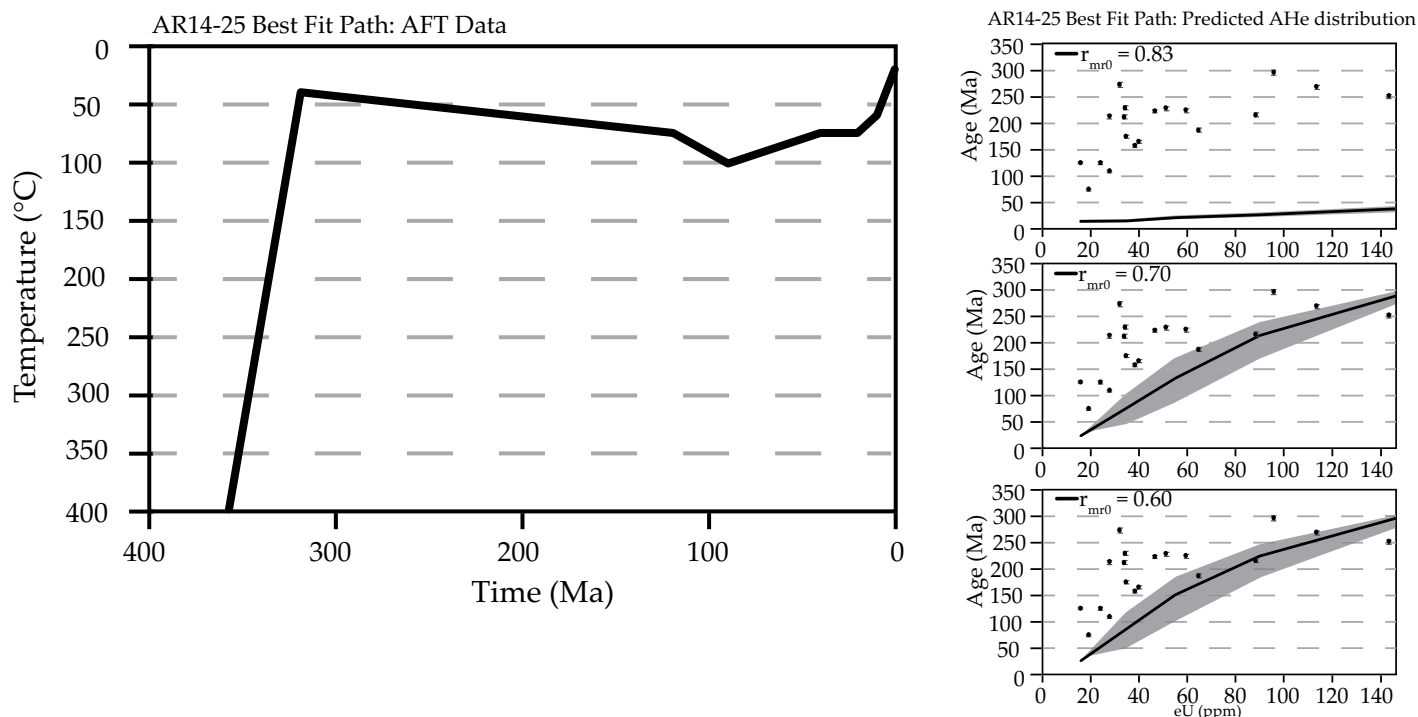
Figure 7. Step 3 of the modeling process evaluates the annealing parameter (r_{mr0}) value that best fits the observed apatite helium (AHe) data given a time-temperature history constrained by Steps 1 and 2. A simplified best fit path from the apatite fission track (AFT) inverse models is shown in the time-temperature history on the left. The right diagram shows envelopes of predicted AHe ages for the same time-temperature history with three different r_{mr0} values. Observed data is indicated by black circles. Values of r_{mr0} of 0.60 best fit the observed data.

For the AHe system, maximum heating of 95 °C best fits the data points (Fig. 8).

The thermal history distilled from the age-eU distribution of AHe data in Step 4 poorly fits the original AFT data. However, the difference between the best fit thermal paths for the AFT and AHe system are only minimal as seen in Figure 9. Whereas the AFT system requires maximum Cretaceous reheating to 100 °C, the AHe system better fits cooling to 95 °C. Similarly, the residence temperature from 40 to 20 Ma is 75 °C for the AFT system and 70 °C for the AHe system. These ±5 °C differences do not change our geologic interpretation of the thermal history of the Sierra de Velasco. Protracted cool conditions from Carboniferous time that persisted throughout the early Cretaceous were terminated in the mid-Cretaceous by a 60 ± 5 °C temperature increase that peaked at ca. 90 Ma. Cooling through the early Paleogene was followed by episodic cooling initiating at 20 Ma and accelerating at 10 Ma.

Samples collected from the vertical transect along the hanging wall of the Velasco Fault come from different structural depths. For this reason, samples from the vertical transect must be modeled independently. However, a single sample typically does not produce apatite grains with the range of eU values (~50 ppm) that

make thermal modeling of AHe samples most effective. One sample does meet this criterion. Sample VEL-06 located at the base of the vertical transect contains AHe samples with a ~50 ppm spread of eU values. Additionally, this sample contains the only Miocene AFT cooling age, 18.6 ± 2.2 Ma, suggesting a difference in the thermal history of this sample. We use the workflow outlined above to model this sample. This sample also required modification of the r_{mr0} value (we used 0.6) to produce a thermal history that satisfies both the AFT and AHe data. We use track length distributions to further evaluate the goodness of fit of forward models (Fig. 10). The results, shown in Figure 10, suggest that this sample reached temperatures between 100 °C and 120 °C by 90 Ma. Like the apatite thermochronometers from the eastern side of the western ridge of the Sierra de Velasco, the AFT and AHe systems have slightly different best fit thermal histories (Figs. 9 and 10); however, the minor differences in these thermal histories do not produce significantly different geologic interpretations. The best fit AFT path requires slow cooling from 120 °C to 80 °C between 90 and 20 Ma. The best fit AHe model indicates faster cooling to 80 °C from 100 to 40 Ma and steady-state thermal conditions from 40 to 20 Ma. Both AFT and AHe models for this sample support

rapid exhumation from 80 °C to surface temperatures at 5 Ma. This sample experienced slightly higher ~20 °C temperatures than the samples from the eastern ridge of the western ridge of Sierra de Velasco, but this difference is consistent with the lower structural depth of this sample.

MODIFICATION OF r_{mr0} Value

In this study, the cooling ages from AHe and AFT grains in the same sample could not be rectified in a common thermal history without the modification of the r_{mr0} value. Our alteration of this value serves as an important contribution to a growing body of evidence that r_{mr0} values can vary significantly across samples (Gautheron et al., 2013; Fox and Shuster, 2014). Appropriate modification of this value is critical to reproduce accurate time-temperature histories that have important implications for thermal and tectonic processes.

The magnitude of the inversion of the AHe and AFT cooling dates used in this study required an evaluation of the effects of chemical and kinetic properties of apatites in AHe dating. The cooling date of an AHe sample is a function of grain size, eU, and apatite annealing kinetics (Farley et al., 1996; Farley, 2000; Flowers et al., 2009). The RDAAM model (Flowers et al.,
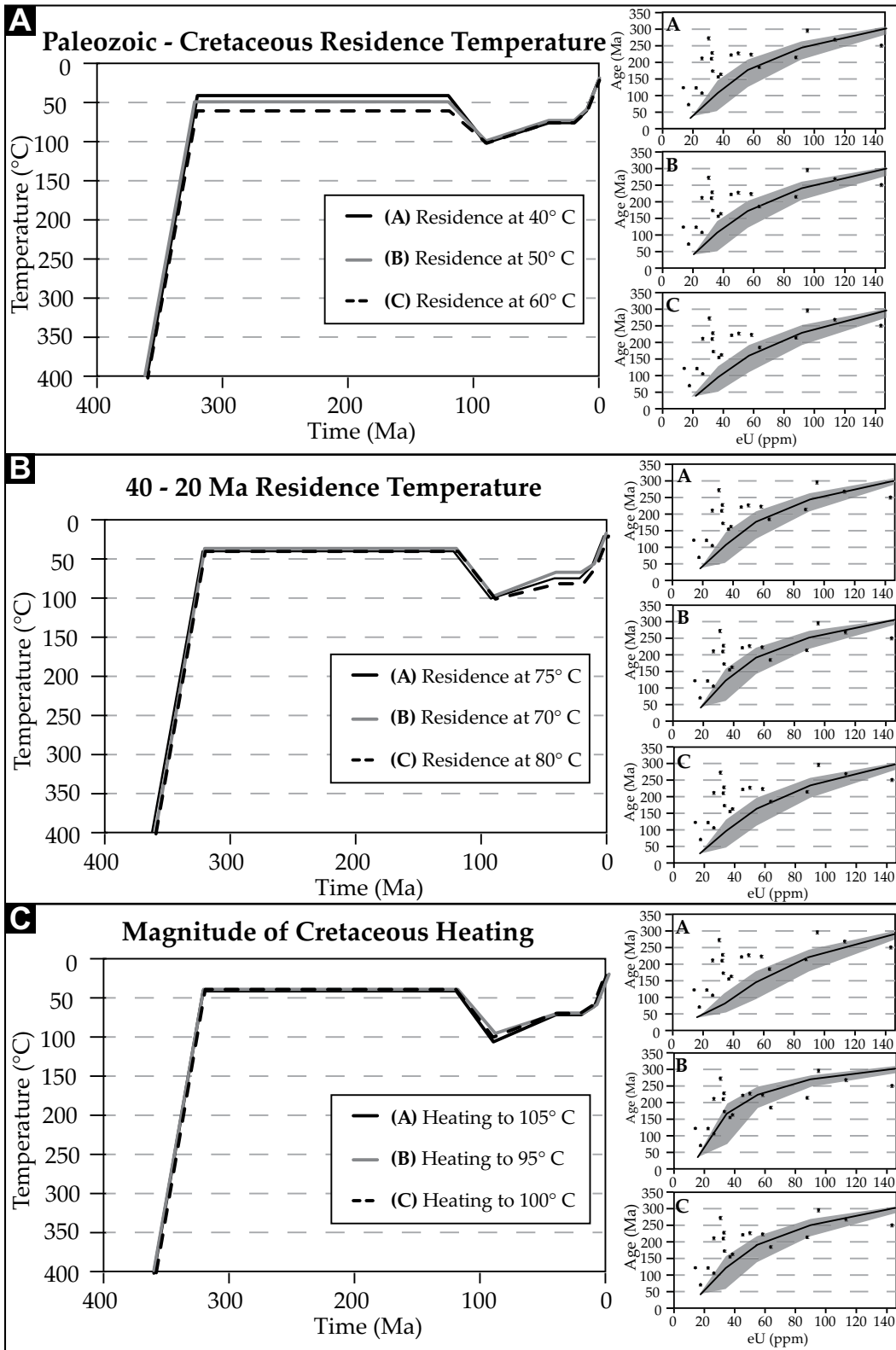
Figure 8. Step 4 of the modeling processes evaluates the effects of three minor modifications (±5–10 °C) to the time-temperature history constrained by Steps 1–3. These modifications address the Paleozoic–Cretaceous residence temperature (A), the 40–20 Ma residence temperature (B), and the magnitude of Cretaceous heating (C). Diagrams on the left show time-temperature histories for each modification (A–C) that corresponds with the diagrams on the right showing the predicted envelopes of apatite helium (AHe) cooling ages for varying effective uranium concentration (eU) values. Observed AHe data is shown by black circles.
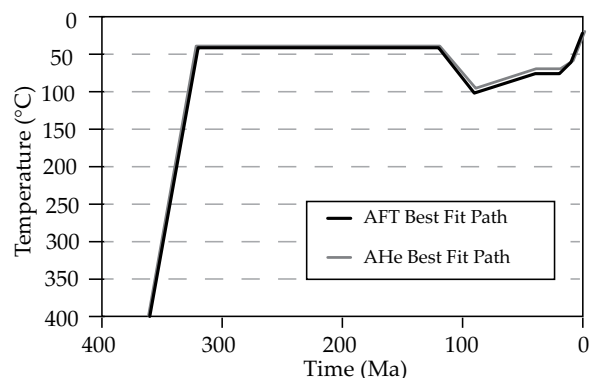
Figure 9. Best fit temperature history for eastern side of the western branch of the Sierra de Velasco for the apatite fission track (AFT) (black line) and apatite helium (AHe) (gray line) systems.

2009) in this study assumes that damage accumulated due to alpha recoil anneals like the damage induced by fission, which is a function of composition. Cl content weakly correlates with the annealing parameter D_{par} in the AFT system, although most studies indicate that Cl content does not independently predict fission annealing kinetics in apatite (Green et al., 1986; Carlson et al., 1999; Ketcham et al., 2007a). The D_{par} measurements for samples from the Sierra de Velasco range from 1.69 to 2.49 µm which correspond to r_{mr0} values above 0.80 as calibrated by the AFT system (Ketcham et al., 2007b). Other authors identify data sets where alpha recoil damage likely does not follow models for fission track annealing, effectively raising the closure temperature of the AHe chronometer even after periods of reheating and presumed healing (Fox and Shuster, 2014; Winn et al., 2017; Fox et al., 2017). Assuming this is the case, samples with thermal histories punctuated by multiple heating and cooling episodes may not reset or only partially reset the AHe chronometer while allowing the AFT system to be completely reset (Gautheron et al., 2013; Fox and Shuster, 2014; Winn et al., 2017; Fox et al., 2017).

The annealing parameter, r_{mr0}, is used in AHe modeling to control the annealing rate of crystal damage caused by the decay of U and Th through alpha recoil and fission. Some evidence indicates that the chemistry of the grain, and specifically Cl content, controls the change in this value (Gautheron et al., 2013). Apatite grains with low eU values (<30 ppm) may be particularly susceptible to differences in r_{mr0} values where extremely low r_{mr0} values increase the AHe date for these grains by greater than 10% (Gautheron et al., 2013). These conditions may be predicted by Cl content of >0.4 wt%. However, the samples in this study had Cl content far below 0.4 wt% and thus did not justify adjusting the r_{mr0} value on this condition.

In summary, neither D_{par} values nor Cl content clearly explain the low r_{mr0} observed in AHe

samples from the Sierra de Velasco. Despite the absence of these supporting data, lowering the r_{mr0} value provides the only time-temperature path that satisfies both AFT and AHe data sets from the Sierra de Velasco. These results have two important implications: first, these data suggest that factors beyond grain chemistry may control the annealing of alpha recoil damage in samples exposed to moderate to low temperature for hundreds of millions of years; second, apatite grains exposed to temperatures within or below the partial annealing zone for hundreds of millions of years accumulate alpha recoil damage that cannot be healed at temperatures as high as ~120–100 °C, which correspond to the closure temperature of the AFT samples analyzed in this study.

DISCUSSION

Interpretation of Thermal History

Together, data from the AFT and the AHe systems used in our thermal models provide a comprehensive history of the thermal evolution of the Sierra de Velasco after emplacement and cooling of Lower Carboniferous plutons. Unlike most previous thermal modeling in the Sierras Pampeanas (Löbens et al., 2011; Bense et al., 2013; Löbens et al., 2013b) the design of both inverse and forward models in this study permit non-monotonic cooling. Exploring non-monotonic cooling paths is critical to account for this complex thermal history. To resolve the large scatter of AHe dates, it is necessary for these samples to spend protracted time—on the order of 100s of millions of years—in the PRZ from ca. 320–120 Ma. During this time, samples were exposed to temperatures no higher than 60 °C. This long term residence in the PRZ creates the radiation damage that is required to increase closure temperature of the AHe system and provide cooling dates older than AFT cooling dates. The AFT system requires a thermal event in the Cretaceous that reset a majority of samples ex-

posed today at the surface. Heating in Cretaceous time to temperatures of 100 ± 5 °C on the eastern side of the western ridge of the Sierra de Velasco, are sufficient to reset the AFT system, but only partially reset the AHe dates throughout the Sierra de Velasco and is followed by cooling in the Late Cretaceous–Paleocene. Miocene exhumation is recorded in the AFT dates of only one sample located at the lowest elevations of the Sierra de Velasco. Thermal modeling of this sample also requires protracted exposure to temperatures cooler than 60 °C throughout the Mesozoic (Fig. 10); however, thermal modeling suggests that this sample reached temperatures close to 120 °C followed by slow cooling during the Paleogene. This sample was likely still at temperatures of ~80 °C until the latest Miocene (Fig. 10).

Thermal modeling is useful to identify periods of heating and cooling and provide clues on exhumation history. Heating in the Cretaceous is consistent with elevated paleogeothermal gradient during rifting and sediment burial. Decreases in temperature between 90 and 60 Ma could potentially result from exhumation and erosion resulting from early Cenozoic shortening (Carrapa et al., 2006; Fosdick et al., 2017), and/or a decreasing geothermal gradient following the cessation of rifting. In the case of burial heating, we would expect the thermal conditions to remain at the peak temperature following burial unless the strata were exhumed. However, following the Cretaceous reheating episode on the east side of the western ridge of the Sierra de Velasco the temperature cools to intermediate temperatures between 70 and 75 °C between 90 and 40 Ma. For this reason, we interpret at least part of Cretaceous reheating to represent an increasing geothermal gradient associated with increased heat flow due to rifting. This interpretation is supported by evidence of hydrothermal activity in the range at this time (Grellet-Tinner and Fiorelli, 2010; Fiorelli et al., 2012). We propose that the geothermal gradient relaxed following the cessation of rifting triggering regional cooling. Retention at temperatures of 70–75 °C from 40 to 20 Ma suggests that some sediment burial may have accompanied Late Cretaceous rifting. Final cooling of the samples from the Sierra de Velasco initiated in the Miocene.

Sample VEL-06, taken from the deepest structural level at the base of the Sierra de Velasco transect, likely experienced the most sediment burial in addition to an overburden of basement rocks from the hanging wall. Thermal modeling supports exposure to higher temperatures for sample VEL-06 relative to other samples throughout the Sierra de Velasco including peak temperatures of 120 °C during Cretaceous
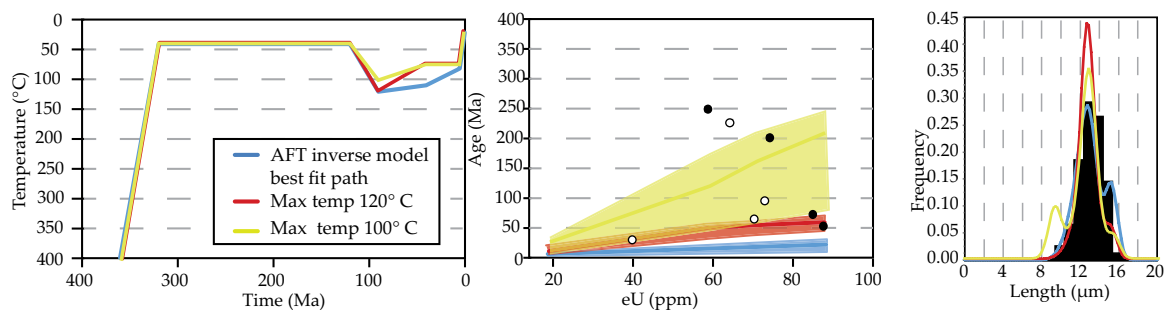
Figure 10. The modeling process outlined in Figure 4 was applied to sample VEL-06 (sample location in Fig. 2A). The final results of this process are shown below. The left diagram shows the best-fit time-temperature histories identified by inverse models of the apatite fission track (AFT) system (blue line) and the best-fit time-temperature histories for the apatite helium (AHe) system with maximum Cretaceous heating of 120 °C (red line) and 100 °C (yellow line). The center diagram shows the predicted envelopes of AHe cooling ages given the three time temperature histories in the left diagram. Measured AHe data is indicated by circles where black circles are grains with a radius >35 μm and white circles are grains with a radius <35 μm. The right diagram shows the predicted AFT length distributions (colored lines) for each of the time temperature histories on the left. The measured AFT length distributions for VEL-06 are shown as a black histogram.

rifting and residence at temperatures between 100 and 80 °C between ca. 60 and 5 Ma. Rapid exhumation at 5 Ma is younger than exhumation modeled for other samples and reflects ongoing exhumation at progressively deeper structural levels.

Temporal Estimates of Granitoid Paleodepths

Limited pre-Cenozoic stratigraphy surrounding the Sierra de Velasco has resulted in a large gap in the regional geologic record; however in a vertical transect, we can use elevation as a proxy for the relative structural depth of each sample to interpret the evolution of the range. Thermal modeling allows us to estimate the temperature of our samples at several key time periods. Using the temperature of our samples obtained

through thermal modeling and assumptions about the paleogeothermal gradient we can calculate the thickness of rocks once located on top of our vertical transect. Although evidence for overburden is not evidence of paleotopography, estimates of both sedimentary and igneous rocks that have been removed from the Sierra de Velasco constrain plausible estimates of paleotopography.

To simplify our calculations, we project the samples taken from the vertical transect at Anillaco onto a single column (Fig. 11). This is consistent with the restoration of basement blocks in this part of the Sierra de Velasco since the Miocene outlined by Larrovere et al. (2016). We exclude sample VEL-01 taken from the top of the range because it is offset by a major fault (Fig. 3). Projecting these samples onto a single column assumes that when the AFT and AHe

samples passed through their respective closure temperatures, the isotherms representing these closure temperatures did not bend significantly. The wavelength of modern topography, ~30 km, and the closure temperatures of both systems suggest this is a reasonable assumption (Reiners, 2007). The difference in elevation between the top (VEL-02) and bottom (VEL-06) samples from the vertical transect is 1.8 km. We call this the preserved section (Fig. 11). We use the thermal histories of the preserved section derived from thermochronology cooling ages and thermal modeling, as well as a range of reasonable assumptions about the paleogeothermal gradient and surface temperature to calculate the thickness of the column of rock removed from on top of the preserved section for key periods of time. These assumptions and calculations are summarized in Table 2.
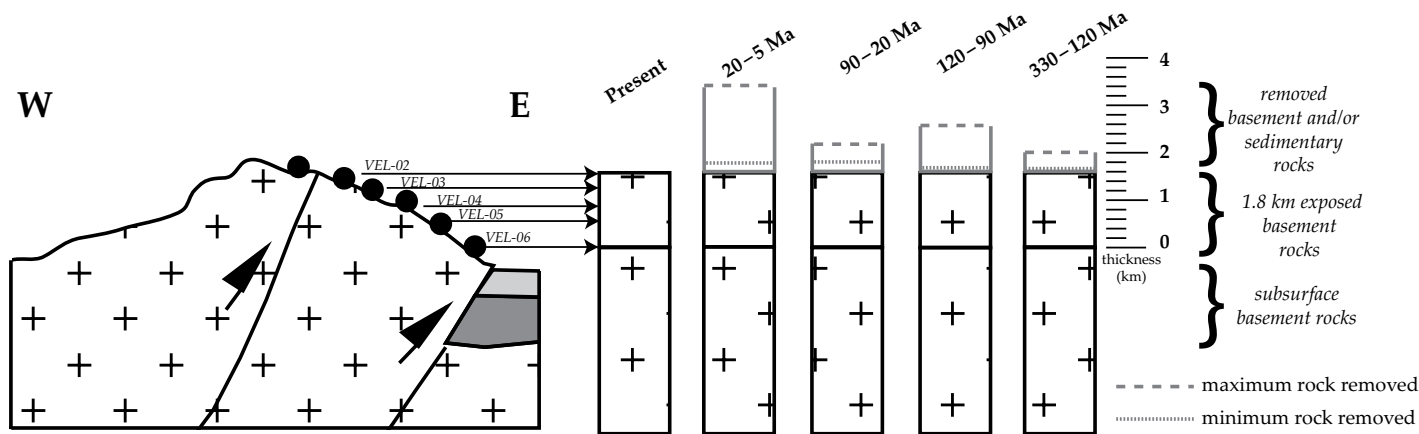

Figure 11. Temporal estimates of granitoid paleodepths can be calculated using the results from thermal modeling. Calculations are described in the text.

TABLE 2. MINIMUM ROCK ERODED FROM SIERRA DE VELASCO

Time period (Ma)	Interpreted event	Thermal modeling requirement	Maximum surface temperature (°C)	Minimum surface temperature (°C)	Maximum geothermal gradient (°C/km)	Minimum geothermal gradient (°C/km)	Required removed cover	Error
20–5	Rapid exhumation	VEL-06 minimum of 80 °C	20	10	35	25	1.0	0.8
60–20	Thermal relaxation and tectonic quiescence	VEL-05 above maximum 75 °C	20	10	35	25	0.2	0.4
120–90	Rifting produces higher geothermal gradients and sediment burial	VEL-02 between 100° and 120 °C	20	10	50	35	0.5	0.5
330–120	Tectonic quiescence	VEL-06 above 60 °C	20	10	35	25	0.0	0.3

The inversion of the AHe and AFT systems in all samples from the Sierra de Velasco requires that these samples were exposed to temperatures below 60 °C for a protracted period of time. Thermal modeling indicates that all samples from the vertical transect at the Sierra de Velasco were at temperatures below 60 °C between ca. 320 and 120 Ma. We assume a geothermal gradient between 25 °C/km and 35 °C/km and a surface temperature between 10 and 20 °C. Given these conditions, the minimum total rock column must have been at least 1.5 ± 0.3 km thick. Additional rock overburden is unconstrained.

Thermal modeling indicates a period of heating between 120 and 90 Ma. This time interval corresponds to regional rifting along the Andean margin. We assume a higher geothermal gradient of between 35 °C/km and 50 °C/km based on modeled and documented increases in the geothermal gradient during rifting of up to 30 °C/km (Baldwin, 1996; Cloetingh et al., 2013; Balázs et al., 2017). Thermal modeling indicates that during this time the top of the preserved section, sample VEL-02, must have reached temperatures high enough to reset the AFT system, between 100 and 120 °C. These conditions require a total rock column of 2.2 ± 0.5 km which includes up to the 1.0 km of additional rock above the 1.8 km preserved rock column (Fig. 11).

We can apply the same approach to the period of time between the end of peak heating in the Cretaceous and the onset of rapid Neogene cooling, 60–20 Ma. During this time period we know that samples VEL-02 to VEL-05, ~1 km of the preserved section, must have been at temperatures lower than the closure temperature of the AFT system and so could not have been at temperatures higher than ~75 °C. Again, we assume surface temperatures between 10 and 20 °C and a geothermal gradient between 25 °C/km and 35 °C/km (Stevens Goddard and Carrapa, 2017). These conditions require a total minimum rock column above sample VEL-05 of 2.0 ± 0.4 km. Subtracting 1 km, an amount which is still conserved in the preserved rock column, indicates that as much as 1.4 km of additional rock must have been on top of the preserved section during this time (Fig. 11).

Between 20 Ma and 5 Ma, the sample at the base of the preserved section, had to maintain temperatures higher than the closure temperature of the AFT system and could not have been lower than 80 °C. We use a revised estimate of the Miocene geothermal gradient between 25 °C/km and 35 °C/km, significantly higher than previous estimates of between 15 °C/km and 20 °C/km, but consistent with estimates of the modern geothermal gradient from well log data (Dávila and Carter, 2013; Collo et al., 2017; Stevens Goddard and Carrapa, 2017). We assume surface temperatures between 10 and 20 °C. These values require a total minimum rock column above sample VEL-06 of 2.8 ± 0.8 km. This means that in addition to the 1.8 km of the preserved section above sample VEL-06 up to 1.8 km of rock could have been eroded from the top of the section producing a maximum erosion rate of 0.06 mm/yr between 20 and 5 Ma. This rate is consistent with erosion rates of granitoids in other parts of the Andes (Carrapa et al., 2006; Deeken et al., 2006).

Paleogeography of the Sierra de Velasco

By including a reasonable range of assumptions about the regional thermal conditions we conclude that 1 ± 0.8 km of additional rock covered the preserved section (1.8 km) at the Sierra de Velasco in the early Miocene. The sample at the base of the preserved section (VEL-06) must have been located at a structural depth of 2.8 ± 0.8 km. In the case that no paleotopography existed in the Sierra de Velasco (Fig. 12B), structural depth is equal to burial and the sample would have been exposed to temperatures of 84 ± 28 °C between ca. 90 Ma and 20 Ma, assuming a geothermal gradient of 30 ± 5 °C/km (Stevens Goddard and Carrapa, 2017). However, if paleotopography did exist in the Sierra de Velasco in the early Miocene (Fig. 12A), relatively horizontal isotherms—justified in this short wavelength topographic feature (Reiners, 2007)—could have exposed samples at deeper structural depths to much lower temperatures than temperatures associated with burial under a flat early–middle Miocene Sierras Pampeanas region.

Thermal modeling from Sierra de Velasco suggests that the samples in this study were retained at temperatures of ~70 °C between 90 and 20 Ma (Figs. 9 and 10). This temperature is lower, but within error of the model suggesting that the Sierra de Velasco was quasi-flat until uplift in the late Miocene (Fig. 12). Retention at temperatures of ~70 °C fits better with the model of pre-Miocene paleotopography.

Although long-lived paleorelief (since the Ordovician) is not required to explain our thermochronology data, we argue that our data are best explained by persisting Paleozoic relief (Fig. 12). Preserving temperatures below the AHe PRZ for sample VEL-06, which would have been a minimum of 2.8 ± 0.8 km below the surface requires: (1) the absence of both erosion and deposition in the Famatinian arc rocks until the Late Cretaceous and (2) a maximum geothermal gradient of 25 °C/km throughout the Paleozoic and most of the Mesozoic (Fig. 12). In contrast, relief generated in the Paleozoic by displacement along the same faults active in the Miocene would place samples now exposed near the base of Sierra de Velasco nearer surface temperatures.

Sustained paleorelief through the Cenozoic is further supported by Neogene sedimentation patterns. Neogene foreland basin deposits >6 km thick are well documented less than 100 km to the west of the Sierra de Velasco in the Bermejo Basin (e.g., Johnson et al., 1986; Reynolds et al., 1990; Malizia et al., 1995; Jordan et al., 2001; Tripaldi et al., 2001; Carrapa et al., 2008; Fosdick et al., 2017; Stevens Goddard and Carrapa, 2017; Ortíz, 2018). However, outcrop studies, geophysical surveys and gravity analysis of the La Rioja and Pipanaco basins to the east of the Sierra de Velasco show an unconformity between Cretaceous and Pliocene strata (Fisher et al., 2002; Bossi et al., 2007; 2009; Dávila, 2012). The absence of Cenozoic foreland basin stratigraphy east of the Sierra de Velasco suggests that this range and the eastern Sierras Pampeanas region were not connected to the regional foreland basin system to the west. We suggest that low-relief relict topography predating the foreland basin, like that proposed in this study, thus restricted sediment transfer
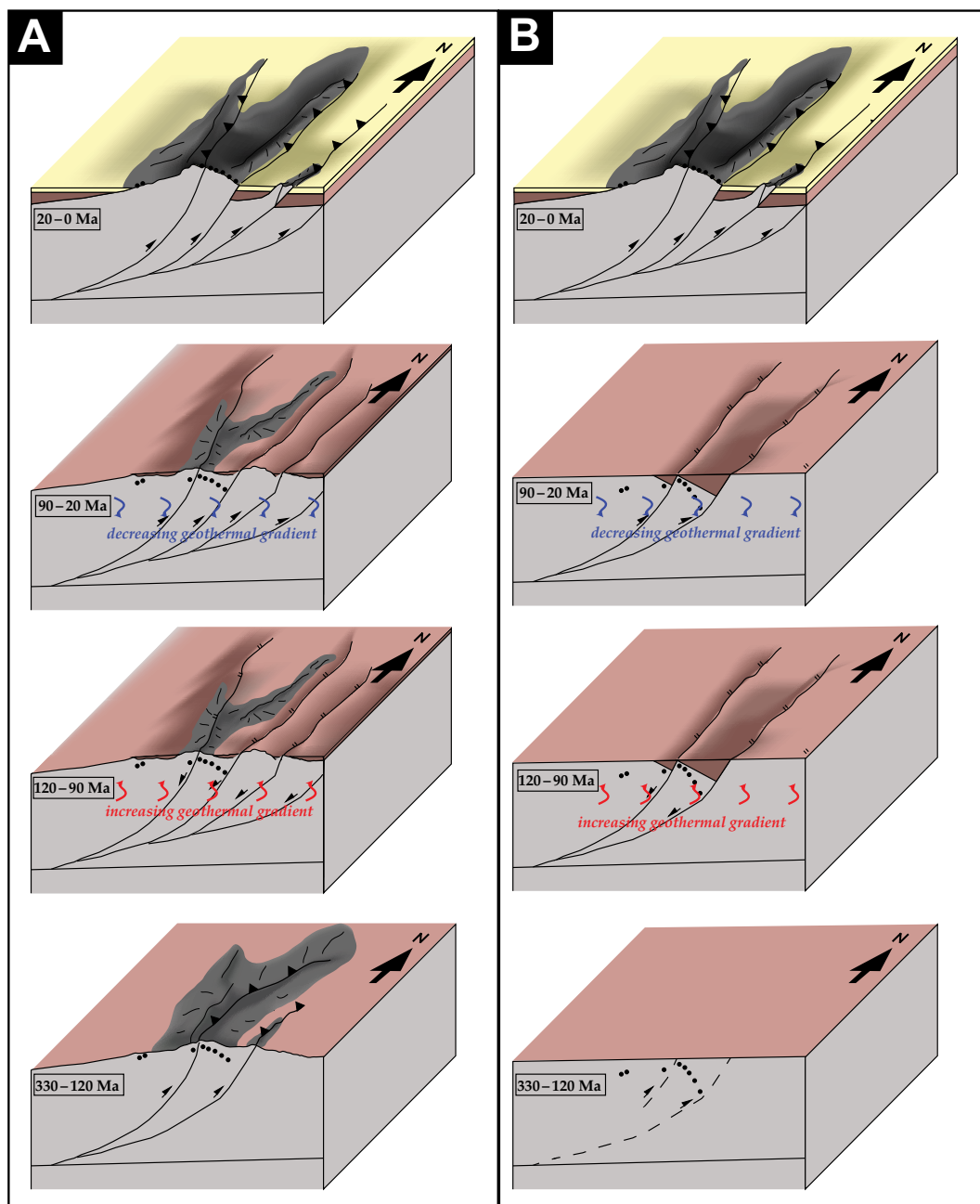
Figure 12. Paleogeographic reconstructions of Sierra de Velasco from the Carboniferous to the present. Locations of samples from the vertical transect are indicated by black circles. (A) Shows a paleogeographic reconstruction assuming some paleotopography is inherited from the Paleozoic, details of this model are discussed in the text. (B) Shows a paleogeographic reconstruction assuming no paleotopography is inherited from the Paleozoic. This model requires several assumptions about the regional geothermal gradient which are discussed in the text.

to the distal foreland to the east. Nearby ranges that experienced even slightly higher reheating events may not preserve the entirety of this thermal history and instead record only Cretaceous or Miocene signals (Coughlin et al., 1998; Sobel and Strecker, 2003; Mortimer et al., 2007; Carrapa et al., 2008; Löbens et al., 2013b). However, it is likely that the regional paleogeography of the Sierras Pampeanas basement block uplifts in the surrounding region experienced a similar history beginning with Ordovician orogenesis, low erosion rates through the late Paleozoic and early Mesozoic, Cretaceous rifting and/or burial, Paleogene cooling and possibly shorten-

ing followed by a period of final exhumation in the Miocene. Future studies in the Sierras Pampeanas will provide an important test of the model supporting long-lived paleotopography by evaluating a similar thermal history in other ranges and reconstructing sediment routing patterns in the Cenozoic foreland basin.

Comparison with Regional Exhumation Models

Measurements of the Miocene geothermal gradient between 25 °C/km and 35 °C/km (Stevens Goddard and Carrapa, 2017) provide new bound-

ary conditions to interpret thermochronological data in the Sierras Pampeanas. Most significantly, this interpretation deviates from previous suggestions by Dávila and Carter (2013) who attribute Permian–Pliocene cooling dates to an extremely low (15–20 °C/km) geothermal gradient. This low geothermal gradient, proposed to develop during flat-slab subduction (Collo et al., 2017), would result in old cooling ages despite exhumation >4 km (Dávila and Carter, 2013).

The thermal modeling results from this study contrast with previous interpretations of the thermal history that do not require a change in the geothermal gradient. This study also does not

identify a period of Jurassic exhumation proposed by Coughlin et al. (1998). It is possible that the AFT cooling ages that are the basis of this previous hypothesis were only partially reset and the cooling age alone only represents a minimum age. Reanalysis of this data set using forward and inverse thermal modeling of multiple thermochronometers should resolve this issue (Ketcham et al., 2007a). Our results and interpretation align with other studies which support long-lived and/or transient paleotopography in the Sierras Pampeanas with evidence of late Paleozoic paleotopography (Jordan et al., 1989), Cretaceous rifting (Bense et al., 2013) followed by various degrees of Cenozoic cooling and exhumation.

Regional Structural Evolution

The structural geology of the Sierra de Velasco is important when considering the interpretation of the cooling ages in the range and within the Sierras Pampeanas. The AFT data produced in this study combined with observed field relationships support the presence of reverse faulting throughout the Sierra de Velasco. Evidence for faulting includes offset in cooling ages where the AFT age in the hanging wall is younger than the AFT age in the footwall. The positive relationship between AFT age and elevation in the Anillaco transect also corroborates our structural interpretation of Sierra de Velasco. Specifically, our structural interpretation of the Sierra de Velasco across the Anillaco transect requires two reverse faults (Fig. 3). Our field measurements combined with evidence from seismic waveform modeling of modern moderate-to-large shallow earthquakes suggests that these faults extend at a high angle, ~44–50°, through basement for 30 km to a regional basement décollement that is interpreted using reprocessed seismic reflection data (Alvarado and Ramos, 2011) and P- and S-seismic wave 1-D crustal models (Venerdini et al., 2016); however, the paucity of sedimentary data bounding the range makes it difficult to test this structural geometry at depth. Alternative structural geometries of the Sierra de Velasco, for example a broad arch with exhumation concentrated at the center of the range, would predict younger cooling dates at higher structural elevations in the range with older cooling dates at lower elevations that experienced less vertical displacement (Braun et al., 2014). This model is not supported by either field measurements or low-temperature thermochronology.

CONCLUSIONS

The integration of multiple thermochronometers with careful thermal modeling provides data that can be used to reconstruct the complex and enigmatic Phanerozoic history of the Sierras Pampeanas. We specifically identify a period from ca. 320 to 120 Ma when nearly all samples in the Sierra de Velasco were at near surface temperatures. Reheating in the Cretaceous was followed by a period of cooling resulting from isothermal relaxation and possibly early Cenozoic shortening and exhumation in Sierra de Velasco. Accelerated late Miocene cooling can be attributed to the initiation of flat slab subduction in the region (Yáñez et al., 2001; Carrapa et al., 2008; Kay and Coira, 2009; Fosdick et al., 2015). Uplift continues today as is evidenced by Quaternary seismic activity (Costa, 2008; Casa et al., 2010; Alvarado and Ramos, 2011). This interpretation is consistent with the timing of regional exhumation in the Sierras Pampeanas suggested by other workers (Sobel and Strecker, 2003; Mortimer et al., 2007; Dávila and Carter, 2013; Löbens et al., 2013b).

The scatter of cooling ages derived from multiple thermochronometers both in this study and throughout the region (Fig. 1) likely reflects a geologic scenario that tests the extreme limits of our current understanding of the kinetic and annealing behavior of the AHe and AFT systems. Thermochronology data produced in the region with only one thermochronometer or without accounting for the effects of radiation damage (Flowers et al., 2009), chemical composition (Gautheron et al., 2013), or annealing parameters such as r_{mr0} (Gautheron et al., 2013; Fox and Shuster, 2014) on the AHe system could not fully capture the record of the regional thermal history.

REFERENCES CITED

Alasino, P.H., Dahlquist, J.A., Pankhurst, R.J., Galindo, C., Casquet, C., Rapela, C.W., Larrovere, M.A., and Fanning, C.M., 2012, Early Carboniferous sub- to mid-alkaline magmatism in the Eastern Sierras Pampeanas, NW Argentina: A record of crustal growth by the incorporation of mantle-derived material in an extensional setting: Gondwana Research, v. 22, p. 992–1008, https://doi.org/10.1016/j.gr.2011.12.011.

Alvarado, P., and Ramos, V.A., 2011, Earthquake deformation in the northwestern Sierras Pampeanas of Argentina based on seismic waveform modelling: Journal of Geodynamics, v. 51, p. 205–218, https://doi.org/10.1016/j.jog.2010.08.002.

Alvarado, P., Beck, S., Zandt, G., Araujo, M., and Triep, E., 2005, Crustal deformation in the south-central Andes backarc terranes as viewed from regional broad-band seismic waveform modelling: Geophysical Journal International, v. 163, p. 580–598, https://doi.org/10.1111/j.1365-246x.2005.02759.x.

Anderson, M., Alvarado, P., Zandt, G., and Beck, S., 2007, Geometry and brittle deformation of the subducting Nazca Plate, Central Chile and Argentina: Geophysical Journal International, v. 171, p. 419–434, https://doi.org/10.1111/j.1365-246X.2007.03483.x.

Ault, A.K., Reiners, P.W., Thomson, S.N., and Miller, G.H., 2015, Inverted Apatite (U-Th)/He and Fission-track Dates from the Rae Craton, Baffin Island, Canada and Implications for Apatite Radiation Damage-He Diffusivity Models, American Geophysical Union Fall Meeting 2015, V32B-04.

Balázs, A., Burov, E., Matenco, L., Vogt, K., Francois, T., and Cloetingh, S., 2017, Symmetry during the syn- and post-rift evolution of the extensional back-arc basins: The role of inherited orogenic structures: Earth and Planetary Science Letters, v. 462, p. 86–98, https://doi.org/10.1016/j.epsl.2017.01.015.

Baldwin, S.L., 1996, Contrasting P-T-t Histories for Blueschists from the Western Baja Terrane and the Aegean: Effects of Synsubduction Exhumation and Backarc Extension, *in* Debout, G.E., Scholl, D.W., Kirby, S.H., and Platt, J.P., eds., Subduction: Top to Bottom: American Geophysical Union Geophysical Monograph 96, p. 135–141, https://doi.org/10.1029/GM096p0135.

Bense, F.A., Löbens, S., Dunkl, I., Wemmer, K., and Siegesmund, S., 2013, Is the exhumation of the Sierras Pampeanas only related to Neogene flat-slab subduction? Implications from a multi-thermochronological approach: Journal of South American Earth Sciences, v. 48, p. 123–144, https://doi.org/10.1016/j.jsames.2013.09.002.

Bossi, G.E., Georgieff, S.M., and Vides, M.E., 2007, Arquitectura y paleoambientes de los depósitos fluviales gravosos de la Formación Las Cumbres (Neógeno), en Villa Mervil, La Rioja, Argentina: Latin American Journal of Sedimentology and Basin Analysis, v. 14, p. 53–75.

Bossi, G.E., Georgieff, S.M., Muruaga, C.M., Ibanez, L.M., and Sanagua, J.G., 2009, Los conglomerados sintectonicos de la Formacion Las Cumbres (Plio-Pleistoceno), Sierras Pampeanas de La Rioja y Catamarca, Argentina: Andean Geology, v. 36, p. 172–196, http://dx.doi.org/10.5027/andgeoV36n2-a02.

Braun, J., Simon-Labric, T., Murray, K.E., and Reiners, P.W., 2014, Topographic relief driven by variations in surface rock density: Nature Geoscience, v. 7, p. 534–540, https://doi.org/10.1038/ngeo2171.

Bull, W.B., 1977. The alluvial-fan environment: Progress in Physical Geography, v. 1, p. 222–270, https://doi.org/10.1177/030913337700100202.

Cahill, T., and Isacks, B.L., 1992, Seismicity and Shape of the Subducted Nazca Plate: Journal of Geophysical Research, v. 97, no. B12, p. 17,503–17,529, https://doi.org/10.1029/92JB00493.

Carlson, W.D., Donelick, R.A., and Ketcham, R.A., 1999, Variability of apatite fission-track annealing kinetics: I. Experimental results: American Mineralogist, v. 84, p. 1213–1223, https://doi.org/10.2138/am-1999-0901.

Carrapa, B., Strecker, M.R., and Sobel, E.R., 2006, Cenozoic orogenic growth in the Central Andes: Evidence from sedimentary rock provenance and apatite fission track thermochronology in the Fiambalá Basin, southernmost Puna Plateau margin (NW Argentina): Earth and Planetary Science Letters, v. 247, p. 82–100, https://doi.org/10.1016/j.epsl.2006.04.010.

Carrapa, B., Hauer, J., Schoenbohm, L., Strecker, M.R., Schmitt, A.K., Villanueva, A., and Gomez, J.S., 2008, Dynamics of deformation and sedimentation in the northern Sierras Pampeanas: An integrated study of the Neogene Fiambala basin, NW Argentina: GSA Bulletin, v. 120, p. 1518–1543, https://doi.org/10.1130/B26111.1.

Carrapa, B., Reyes-Bywater, S., Safipour, R., Sobel, E.R., Schoenbohm, L.M., DeCelles, P.G., Reiners, P.W., and

Stockli, D., 2014, The effect of inherited paleotopography on exhumation of the Central Andes of NW Argentina: GSA Bulletin, v. 126, p. 66–77, https://doi.org/10.1130/B30844.1.

Casa, A.L., Yamin, M.G., Cegarra, M.I., Coppolecchia, M., and Costa, C.H., 2010, Deformación cuaternaria asociada al frente de levantamiento oriental de las Sierras de Velasco y Ambato: Revista de la Asociación Geológica Argentina, v. 67, p. 425–438.

Ciccioli, P.L., Limarino, C.O., Marenssi, S.A., Tedesco, A.M., and Tripaldi, A., 2011, Tectosedimentary evolution of the La Troya and Vinchina depocenters (northern Bermejo Basin, Tertiary), La Rioja, Argentina: Cenozoic Geology of the Central Andes of Argentina, p. 91–110.

Cloetingh, S., Burov, E., Matenco, L., Beekman, F., Roure, F., Ziegler, P., 2013, The Moho in extensional tectonic settings: Insights from thermo-mechanical models: Tectonophysics, v. 609, p. 558–604, https://doi.org/10.1016/j.tecto.2013.06.010.

Collo, G., Dávila, F.M., Teixeira, W., Nóbile, J.C., Anna, L.S., and Carter, A., 2017, Isotopic and thermochronologic evidence of extremely cold lithosphere associated with a slab flattening in the Central Andes of Argentina: Basin Research, https://doi.org/10.1111/bre.12163.

Costa, C., 2008, Neotectónica, *in* Peligrosidad sísmica en la Sierra de Velasco: SEGEMAR, Serie Contribuciones Técnicas Nro. 14, p. 30–73.

Coughlin, T.J., O'Sullivan, P.B., Kohn, B.P., and Holcombe, R.J., 1998, Apatite fission-track thermochronology of the Sierra Pampeanas, central western Argentina: Implications for the mechanism of plateau uplift in the Andes: Geology, v. 26, p. 999–1002, https://doi.org/10.1130/0091-7613(1998)026<0999:AFTTOT>2.3.CO;2.

Dahlquist, J.A., Pankhurst, R.J., Gaschnig, R.M., Rapela, C.W., Casquet, C., Alasino, P.H., Galindo, C., and Baldo, E.G., 2013, Hf and Nd isotopes in Early Ordovician to Early Carboniferous granites as monitors of crustal growth in the Proto-Andean margin of Gondwana: Gondwana Research, v. 23, p. 1617–1630, https://doi.org/10.1016/j.gr.2012.08.013.

Dávila, F.M., and Astini, R.A., 2007, Cenozoic provenance history of synorogenic conglomerates in western Argentina (Famatina belt): Implications for Central Andean foreland development: GSA Bulletin, v. 119, p. 609–622, https://doi.org/10.1130/B26007.1.

Dávila, F.M., and Carter, A., 2013, Exhumation history of the Andean broken foreland revisited: Geology, v. 41, p. 443–446, https://doi.org/10.1130/G33960.1.

Dávila, F.M., Astini, R.A., Jordan, T.E., and Kay, S.M., 2004, Early Miocene andesite conglomerates in the Sierra de Famatina, broken foreland region of western Argentina, and documentation of magmatic broadening in the south Central Andes: Journal of South American Earth Sciences, v. 17, p. 89–101, https://doi.org/10.1016/j.jsames.2004.04.001.

Dávila, F.M., Giménez, M.E., Nóbile, J.C., and Martínez, M.P., 2012, The evolution of high-elevated depocenters of the northern Sierras Pampeanas (ca. 28° SL), Argentine broken foreland, South-Central Andes: The Pipanaco Basin: Basin Research, v. 24, p. 615–636, https://doi.org/10.1111/j.1365-2117.2011.00539.x.

Deeken, A., Sobel, E.R., Coutand, I., Haschke, M., Riller, U., and Strecker, M.R., 2006, Development of the southern Eastern Cordillera, NW Argentina, constrained by apatite fission track thermochronology: From early Cretaceous extension to middle Miocene shortening: Tectonics, v. 25, https://doi.org/10.1029/2005TC001894.

de los Hoyos, C.R., Willner, A.P., Larrovere, M.A., Rossi, J.N., Toselli, A.J., and Basei, M.A.S., 2011, Tectonothermal evolution and exhumation history of the Paleozoic Proto-Andean Gondwana margin crust: The Famatinian Belt in NW Argentina: Gondwana Research, v. 20, p. 309–324, https://doi.org/10.1016/j.gr.2010.12.004.

Donelick, R.A., Ketcham, R.A., and Carlson, W.E., 1999, Variability of apatite fission-track annealing kinetics: II. Crystallographic orientation effects: American Mineralogist, v. 84, p. 1224–1234, https://doi.org/10.2138/am-1999-0902.

Ehlers, T.A., and Farley, K.A., 2003, Apatite (U-Th)/He thermochronometry: Methods and applications to problems in tectonic and surface processes: Earth and Planetary Science Letters, v. 206, p. 1–14, https://doi.org/10.1016/S0012-821X(02)01069-5.

Enkelmann, E., Ridgway, K.D., Carignano, C., and Linnemann, U., 2014, A thermochronometric view into an ancient landscape: Tectonic setting, development, and inversion of the Paleozoic eastern Paganzo basin, Argentina: Lithosphere, v. 6, p. 93–107, https://doi.org/10.1130/L309.1.

Farley, K.A., 2000, Helium diffusion from apatite: General behavior as illustrated by Durango fluorapatite: Journal of Geophysical Research, v. 105, p. 2903–2914, https://doi.org/10.1029/1999JB900348.

Farley, K.A., Wolf, R.A., and Silver, L.T., 1996, The effects of long alpha-stopping distances on (U-Th)/He ages: Geochimica et Cosmochimica Acta, v. 60, p. 4223–4229, https://doi.org/10.1016/S0016-7037(96)00193-7.

Fernandez-Seveso, F., and Tankard, A.J., 1995, Tectonics and stratigraphy of the Late Paleozoic Paganzo Basin of Western Argentina and its regional implications, *in* Tankard, A.J., Suarez, S., and Welsink, H.J., eds., Petroleum Basins of South America: AAPG Memoir, v. 62, p. 285–301.

Fiorelli, L.E., Grellet-Tinner, G., Alasino, P.H., and Argañaraz, E., 2012, The geology and palaeoecology of the newly discovered Cretaceous neosauropod hydrothermal nesting site in Sanagasta (Los Llanos Formation), La Rioja, northwest Argentina: Cretaceous Research, v. 35, p. 94–117, https://doi.org/10.1016/j.cretres.2011.12.002.

Fisher, N.D., Jordan, T.E., and Brown, L., 2002, The structural and stratigraphic evolution of the La Rioja basin, Argentina: Journal of South American Earth Sciences, v. 15, p. 141–156, https://doi.org/10.1016/S0895-9811(02)00010-X.

Fleischer, R.L., Price, P.B., and Walker, R.M., 1975, Nuclear Tracks in Solids: Principles and Applications: Berkeley, California, USA, University of California Press, 605 p.

Flowers, R.M., Ketcham, R.A., Shuster, D.L., and Farley, K.A., 2009, Apatite (U–Th)/He thermochronometry using a radiation damage accumulation and annealing model: Geochimica et Cosmochimica Acta, v. 73, p. 2347–2365, https://doi.org/10.1016/j.gca.2009.01.015.

Fosdick, J.C., Carrapa, B., and Ortiz, G., 2015, Faulting and erosion in the Argentina Precordillera during changes in subduction regime: Reconciling bedrock cooling and detrital records: Earth and Planetary Science Letters, v. 432, p. 73–83, https://doi.org/10.1016/j.epsl.2015.09.041.

Fosdick, J.C., Reat, E.J., Carrapa, B., Ortiz, G., and Alvarado, P.M., 2017, Retroarc basin reorganization and aridification during Paleogene uplift of the southern central Andes: Tectonics, v. 36, https://doi.org/10.1002/2016TC004400.

Fox, M., and Shuster, D.L., 2014, The influence of burial heating on the (U–Th)/He system in apatite: Grand Canyon case study: Earth and Planetary Science Letters, v. 397, p. 174–183, https://doi.org/10.1016/j.epsl.2014.04.041.

Fox, M., Tripathy-Lang, A., Shuster, D.L., Winn, C., Karlstrom, K., and Kelley, K., 2017, Westernmost Grand Canyon incision: Testing thermochronometric resolution: Earth and Planetary Science Letters, v. 474, p. 248–256, https://doi.org/10.1016/j.epsl.2017.06.049.

Galliski, M.A., and Viramonte, J.G., 1988, The Cretaceous paleorift in northwestern Argentina: A petrologic approach: Journal of South American Earth Sciences, v. 1, p. 329–342, https://doi.org/10.1016/0895-9811(88)90021-1.

Gautheron, C., Barbarand, J., Ketcham, R.A., Tassan-Got, L., van der Beek, P., Pagel, M., Pinna-Jamme, R., Couffignal, F., and Fialin, M., 2013, Chemical influence on α-recoil damage annealing in apatite: Implications for (U–Th)/He dating: Chemical Geology, v. 351, p. 257–267, https://doi.org/10.1016/j.chemgeo.2013.05.027.

González Bonorino, F., 1950, Algunos problemas geológicos de las Sierras Pampeanas: Revista de la Asociación Geológica Argentina, v. 5, no. 3, p. 81–110.

González Bonorino, F., 1972, Descripción Geológica de la Hoja 13c, "Fambalá" (Provincia de Catamarca): Dirección Nacional de Geología y Minería, Buenos Aires, Argentina: Boletin-Instituto de Estudios de Poblacion y Desarrollo (Dominican Republic), v. 127, p. 1–73.

Green, P.F., Duddy, I.R., Gleadow, A.J.W., Tingate, P.R., and Laslett, G.M., 1986, Thermal annealing of fission tracks in apatite: 1. A qualitative description: Chemical Geology: Isotope Geoscience section, v. 59, p. 237–253, https://doi.org/10.1016/0168-9622(86)90074-6.

Green, P.F., Duddy, I.R., Laslett, G.M., Hegarty, K.A., Gleadow, A.J.W., and Lovering, J.F., 1989, Thermal annealing of fission tracks in apatite 4. Quantitative modelling techniques and extension to geological timescales: Chemical Geology: Isotope Geoscience section, v. 79, p. 155–182, https://doi.org/10.1016/0168-9622(89)90018-3.

Grellet-Tinner, G., and Fiorelli, L.E., 2010, A new Argentinean nesting site showing neosauropod dinosaur reproduction in a Cretaceous hydrothermal environment: Nature Communications, v. 1, p. 1–8, https://doi.org/10.1038/ncomms1031.

Grosse, P., Bellos, L.I., de los Hoyos, C.R., Larrovere, M.A., Rossi, J.N., and Toselli, A.J., 2011, Across-arc variation of the Famatinian magmatic arc (NW Argentina) exemplified by I-, S- and transitional I/S-type Early Ordovician granitoids of the Sierra de Velasco: Journal of South American Earth Sciences, v. 32, p. 110–126, https://doi.org/10.1016/j.jsames.2011.03.014.

Johnson, N.M., Jordan, T.E., Johnsson, P.A., and Naeser, C.W., 1986, Magnetic polarity stratigraphy, age and tectonic setting of fluvial sediments in an eastern Andean foreland basin, San Juan Province, Argentina, *in* Allen, P.A., and Homewood, P., eds., Foreland Basins: London, Blackwell Science Publications, p. 63–75.

Jordan, T.E., and Allmendinger, R.W., 1986, The Sierras Pampeanas of Argentina; a modern analogue of Rocky Mountain foreland deformation: American Journal of Science, v. 286, p. 737–764, https://doi.org/10.2475/ajs.286.10.737.

Jordan, T.E., Isacks, B.L., Allmendinger, R.W., Brewer, J.A., Ramos, V.A., and Ando, C.J., 1983, Andean tectonics related to geometry of subducted Nazca plate: Geological Society of America Bulletin, v. 95, no. 7, p. 341–361, https://doi.org/10.1130/0016-7606(1983)94<341:ATRTGO>2.0.CO;2.

Jordan, T.E., Zeitler, P., Ramos, V., and Gleadow, A.J.W., 1989, Thermochronometric data on the development of the basement peneplain in the Sierras Pampeanas, Argentina: Journal of South American Earth Sciences, v. 2, p. 207–222, https://doi.org/10.1016/0895-9811(89)90030-8.

Jordan, T.E., Schlunegger, F., and Cardozo, N., 2001, Unsteady and spatially variable evolution of the Neogene Andean Bermejo foreland basin, Argentina: Journal of South American Earth Sciences, v. 14, p. 775–798, https://doi.org/10.1016/S0895-9811(01)00072-4.

Kay, S.M., and Coira, B.L., 2009, Shallowing and steepening subduction zones, continental lithospheric loss, magmatism, and crustal flow under the Central Andean Altiplano-Puna Plateau, *in* Kay, S.M., Ramos, V.A., and Dickinson, W.R., eds., Backbone of the Americas: Shallow Subduction, Plateau Uplift, and Ridge and Terrane Collision: Geological Society of America, v. 204, p. 229–259, https://doi.org/10.1130/2009.1204(11).

Ketcham, R.A., 2005, Forward and Inverse Modeling of Low-Temperature Thermochronometry Data: Reviews in Mineralogy and Geochemistry, v. 58, p. 275–314, https://doi.org/10.2138/rmg.2005.58.11.

Ketcham, R.A., Carter, A., Donelick, R.A., Barbarand, J., and Hurford, A.J., 2007a, Improved modeling of fission-track annealing in apatite: American Mineralogist, v. 92, p. 799–810, https://doi.org/10.2138/am.2007.2281.

Ketcham, R.A., Carter, A., Donelick, R.A., Barbarand, J., and Hurford, A.J., 2007b, Improved measurement of fission-track annealing in apatite using c-axis projection: American Mineralogist, v. 92, p. 789–798, https://doi.org/10.2138/am.2007.2280.

Ketcham, R.A., Gautheron, C., and Tassan-Got, L., 2011, Accounting for long alpha-particle stopping distances in (U-Th-Sm)/He geochronology: Refinement of the baseline case: Geochimica et Cosmochimica Acta, v. 75, p. 7779–7791.

Larrovere, M., Alasino, P.H., and Baldo, E.G., 2016, La faja de cizalla dúctil doble-vergente del noroeste de la sierra de Velasco: Deformación de la corteza media durante la orogenia Famatiniana: Revista de la Asociación Argentina, v. 73, p. 117–133.

Löbens, S., Bense, F.A., Wemmer, K., and Dunkl, I., 2011, Exhumation and uplift of the Sierras Pampeanas: Preliminary implications from K–Ar fault gouge dating and low-T thermochronology in the Sierra de Comechingones (Argentina): International Journal of Earth Science, v. 100, p. 671–694.

Löbens, S., Bense, F.A., Dunkl, I., Wemmer, K., Kley, J., and Siegesmund, S., 2013a, Thermochronological constraints of the exhumation and uplift of the Sierra de Pie de Palo, NW Argentina: Journal of South American Earth Sciences, v. 48, p. 209–219, https://doi.org/10.1016/j.jsames.2013.09.005.

Löbens, S., Sobel, E.R., Bense, F.A., Wemmer, K., Dunkl, I., and Siegesmund, S., 2013b, Refined exhumation history of the northern Sierras Pampeanas, Argentina: Tectonics, v. 32, p. 453–472, https://doi.org/10.1002/tect.20038.

Malizia, D.C., Reynolds, J.H., and Tabbutt, K.D., 1995, Chronology of Neogene sedimentation, stratigraphy, and tectonism in the Campo de Talampaya region, La Rioja Province, Argentina: Sedimentary Geology, v. 96, p. 231–255, https://doi.org/10.1016/0037-0738(94)00132-E.

Mortimer, E., Carrapa, B., Coutand, I., Schoenbohm, L., Sobel, E.R., Gomez, J.S., and Strecker, M.R., 2007, Fragmentation of a foreland basin in response to out-of-sequence basement uplifts and structural reactivation: El Cajon-Campo del Arenal basin, NW Argentina: GSA Bulletin, v. 119, p. 637–653, https://doi.org/10.1130/B25884.1.

Ortíz, G., 2018, Deformación Andina en el Extremo Norte de La Sierra de Valle Fértile: Un Estudio Integrado Basado en Termocronología y Geofísica [Ph.D. thesis]: Universidad Nacional de San Juan, Argentina, 162 p.

Ortíz, G., Alvarado, P., Fosdick, J.C., Perucca, L., Saez, M., and Venerdini, A., 2015, Active deformation in the northern Sierra de Valle Fértil, Sierras Pampeanas, Argentina: Journal of South American Earth Sciences, v. 64, p. 339–350, https://doi.org/10.1016/j.jsames.2015.08.015.

Pieroni, E.M., and Georgieff, S.M., 2007, Reconsideración estratigráfica del Neopaleozoico de los alrededores del dique Los Sauces, La Rioja: Revista de la Asociación Geológica Argentina, v. 62, p. 105–115.

Price, P.B., and Walker, R.M., 1963, Fossil tracks of charged particles in mica and the age of minerals: Journal of Geophysical Research, v. 68, p. 4847–4862, https://doi.org/10.1029/JZ068i016p04847.

Ramos, V.A., Cristallini, E.O., and Pérez, D.J., 2002, The Pampean flat-slab of the Central Andes: Journal of South American Earth Sciences, v. 15, p. 59–78, https://doi.org/10.1016/S0895-9811(02)00006-8.

Reiners, P.W., 2007, Thermochronologic Approaches to Paleotopography: Reviews in Mineralogy and Geochemistry, v. 66, p. 243–267, https://doi.org/10.2138/rmg.2007.66.10.

Reyes, F.C., and Salfity, J.A., 1973, Consideraciones sobre la estratigrafía del Cretácico (Subgrupo Pirgua) del noroeste Argentino: V Congreso Geológico Argentino, v. 3, p. 355–385.

Reynolds, J.H., Jordan, T.E., Johnson, N.M., Damanti, J.F., and Tabbutt, K.D., 1990, Neogene deformation of the flat-slab subduction segment of the Argentine-Chilean Andes: Magnetostratigraphic constraints from Las Juntas, La Rioja province, Argentina: GSA Bulletin, v. 102, p. 1607–1622, https://doi.org/10.1130/0016-7606(1990)102<1607:NDOTFS>2.3.CO;2.

Richardson, T., Ridgway, K.D., Gilbert, H., Martino, R., Enkelmann, E., Anderson, M., and Alvarado, P., 2013, Neogene and Quaternary tectonics of the Eastern Sierras Pampeanas, Argentina: Active intraplate deformation inboard of flat-slab subduction: Tectonics, v. 32, p. 780–796, https://doi.org/10.1002/tect.20054.

Salfity, J.A., and Marquillas, R.A., 1994, Tectonic and Sedimentary Evolution of the Cretaceous-Eocene Salta Group Basin, Argentina, *in* Salfity, J.A., ed., Cretaceous Tectonics of the Andes, Vieweg Publishing, Wiesbaden, Germany, p. 266–315, https://doi.org/10.1007/978-3-322-85472-8_6.

Schmidt, C.J., Astini, R.A., Costa, C.H., Gardini, C.E., and Kraemer, P.E., 1995, Cretaceous rifting, alluvial fan sedimentation, and Neogene inversion, southern Sierras Pampeanas, Argentina, *in* Tankard, A.J., Suarez, S., and Welsink, H.J., eds., Petroleum Basins of South America: AAPG Memoir, v. 62, p. 341–358.

Sobel, E.R., and Strecker, M.R., 2003, Uplift, exhumation and precipitation: Tectonic and climatic control of Late Cenozoic landscape evolution in the northern Sierras Pampeanas, Argentina: Basin Research, v. 15, p. 431–451, https://doi.org/10.1046/j.1365-2117.2003.00214.x.

Stevens Goddard and Carrapa, 2017, Using basin thermal history to evaluate the role of Miocene-Pliocene flat-slab subduction in the southern Central Andes (27°S–30°S): Basin Research, https://doi.org/10.1111/bre.12265.

Tauber, A.A., 2005, Mamíferos fósiles y edad de la Formación Salicas (Mioceno tardío) de la sierra de Velasco, La Rioja, Argentina: Ameghiniana, v. 42, p. 443–460.

Tripaldi, A., Net, L., Limarino, C., Marenssi, S., Ré, G., and Caselli, A., 2001, Paleoambientes sedimentarios y procedencia de la Formación Vinchina, Mioceno, noroeste de la provincia de La Rioja: Revista de la Asociación Geológica Argentina, v. 56, p. 443–465.

Turner, J.C.M., 1971, Descripción Geológica de la Hoja 15d, "Famatina" (Provincia de La Rioja): Dirección Nacional de Geología y Minería, Buenos Aires, Argentina: Boletin—Instituto de Estudios de Poblacion y Desarrollo (Dominican Republic), v. 126, p. 1–96.

Venerdini, A., Sánchez, G., Alvarado, P., Bilbao, I., and Ammirati, J.B., 2016, Nuevas determinaciones de velocidades de ondas P y ondas S para la corteza sísmica del terreno Cuyania en el retroarco andino: Revista Mexicana de Ciencias Geológicas, v. 33, p. 59–71.

Wagner, G.A., Gleadow, A.J.W., and Fitzgerald, P.G., 1989, The significance of the partial annealing zone in apatite fission-track analysis: Projected track length measurements and uplift chronology of the Transantarctic Mountains: Chemical Geology, v. 79, p. 295–305.

Winn, C., Karlstrom, K.E., Shuster, D.L., Kelley, S., and Fox, M., 2017, 6 Ma carving of Westernmost Grand Canyon: Reconciling geologic data with combined AFT, (U-Th)/He, and ⁴He/³He thermochronologic data: Earth and Planetary Science Letters, v. 474, p. 257–271, https://doi.org/10.1016/j.epsl.2017.06.051.

Yáñez, G.A., Ranero, C.R., von Huene, R., and Díaz, J., 2001, Magnetic anomaly interpretation across the southern central Andes (32°–34°S): The role of the Juan Fernández Ridge in the late Tertiary evolution of the margin: Journal of Geophysical Research. Solid Earth, v. 106, p. 6325–6345, https://doi.org/10.1029/2000JB900337.